Progress in Aerospace Sciences 45 (2009) 30–49

Contents lists available at ScienceDirect

Progress in Aerospace Sciences

journal homepage: www.elsevier.com/locate/paerosci

Experimental research in aerodynamic control with electric and electromagnetic fields ☆

E.M. Braun *, F.K. Lu, D.R. Wilson

Department of Mechanical and Aerospace Engineering, Aerodynamics Research Center, University of Texas at Arlington, Arlington, TX 76019, USA

ARTICLE INFO

Available online 7 January 2009

PACS:
47.65.−d
47.85.lb
47.85.ld
52.80.Hc
52.80.Pi

ABSTRACT

Fifty years ago, publications began to discuss the possibilities of electromagnetic flow control (EMFC) to improve aerodynamic performance. This led to an era of research that focused on coupling the fundamentals of magnetohydrodynamics (MHD) with propulsion, control, and power generation systems. Unfortunately, very few designs made it past an exploratory phase as, among other issues, power consumption was unreasonably high. Recent proposed advancements in technology like the MARIAH hypersonic wind tunnel and the AJAX scramjet engine concepts have led to a new phase of MHD research in the aerospace industry, with many interdisciplinary applications. Compared with propulsion systems and channel flow accelerators, EMFC concepts applied to control surface aerodynamics have not seen the same level of advancement that may eventually produce a device that can be integrated with an aircraft or missile. The purpose of this paper is to review the overall feasibility of the different electric and EMFC concepts. Emphasis is placed on EMFC with high voltage ionization sources and experimental work.

Contents

1. Introduction

Fifty years ago, an article was written describing the prospects for "Magneto-Aerodynamics" [1]. In it, Resler and Sears stated that an electromagnetic field could be coupled with an ionized gas flow to accelerate or decelerate it, delay boundary layer separation, or to control skin friction and heat transfer. With several additions since that time, these goals remain the same. The authors also discussed several advancements critical to the progress of electromagnetic flow control (EMFC). Among them was the ability to solve the complex magnetohydrodynamic equations, which has eased tremendously stemming from the development of powerful computing hardware and numerical methodologies. Next, Resler and Sears mentioned that powerful magnets would be needed for ionized fluid flow control. This requirement of high strength magnets has been achieved to some extent. Electromagnets can produce fields of several tesla, and superconducting magnets can reach tens of tesla. However,

☆ An abbreviated version of this paper was presented as AIAA Paper 2008-3788 at the 39th AIAA Plasmadynamics and Lasers Conference, Seattle, Washington, June 23–26, 2008.

* Corresponding author. Tel.: +1 817 272 5120; fax: +1 817 272 5124.
E-mail address: eric.braun@mavs.uta.edu (E.M. Braun).

0376-0421/$ - see front matter © 2008 Elsevier Ltd. All rights reserved.
doi:10.1016/j.paerosci.2008.10.003

Nomenclature

b	induced magnetic field, T
B	magnetic field, T
c_f	skin friction coefficient
DBD	dielectric barrier discharge
E	electric field, V/m
e	electron charge, -1.602×10^{-19} C
EFC	electrohydrodynamic flow control
EMFC	electromagnetic flow control
F	force, N
F_L	Lorentz force, N (single particle), N/m^3 (ionized particles per unit volume)
I	current, A
I_{BL}	$= \sigma B^2 L/\rho u_\infty (c_f/2)^{1/2}$, boundary layer magnetic interaction parameter
I_{EM}	$= BE\sigma L/\rho u^2$, electromagnetic interaction parameter
I_M	$= \sigma B^2 L/\rho u$, magnetic interaction parameter
J	current field, A/m^2
L	characteristic length, m
n	number density, 1/m^3
p	static pressure, Pa
q	electric charge, C
Re_M	$= \mu_0 \sigma u L$, magnetic Reynolds number
r	distance, m
S	cross-sectional area, m^2
u	flow speed, m/s
V	voltage, V
WIG	weakly ionized gas
x	streamwise Cartesian coordinate
y	spanwise Cartesian coordinate
z	transverse Cartesian coordinate
Z	number of net charges on a particle
ε_0	permittivity of vacuum, 8.854×10^{-12} F/m
μ_0	permeability of vacuum, 1.257×10^{-6} N/A^2
ρ	density, kg/m^3
ρ_e	charge density, C/m^3
σ	conductivity, $\mho$/m

Subscripts

BL	boundary layer
p	particle
∞	freestream

the size of these magnets makes their integration into an aerospace vehicle problematic. Also, the magnets are dependent upon large power supplies. Similarly, research into rare-earth materials has progressed considerably since 1958, with inexpensive neodymium-based magnets currently available with maximum surface fields in the 0.5–1.0 T range. However, their use for aerodynamic control is limited since their magnetic fields are reduced as temperature is increased, making their incorporation into applications like scramjet inlets difficult if not impractical.

In addition to the strength of the magnetic field, EMFC is also dependent upon the conductivity of the ionized airflow. Resler and Sears believed that artificial seeding of the airflow to create higher plasma conductivities would need development. At the time, plasma jet sources were capable of creating high values of conductivity for ground testing. As an example, consider a linear Lorentz force accelerator developed in the 1960s [2]. The accelerator had a square cross-section of 2.54 cm sides at the inlet that diverged to about 2.54×5 cm at the exit with an overall length of 76 cm. The 60 electrode pairs in the accelerator were powered by a warehouse of 1700, 12 V automotive batteries. The current draw of the accelerator electromagnets reached up to 900 A at 80 V. Finally, the plasma generator operated with a 10 MW power supply, and could create a flow with a conductivity of up to 500 $\mho$/m (with seeding). Note that units of conductivity are labeled using $\mho$/m which is equal to Ω^{-1}/m. Historically, conductivity has been described using mhos per meter although the unit name siemens (S) has been designated for Ω^{-1} to make $\mho$/m equal to S/m. In order to reduce the power requirement, seeding the plasma jet with low ionization energy potassium and cesium compounds was explored, which resulted in a tremendous increase in conductivity relative to the unseeded gas. For instance, a hypersonic vehicle flying at an altitude of 30 km at Mach 16 would ionize the air after a bow shock to $\sigma \approx 0.05\,\mho$/m. Adding 0.1% potassium by weight could boost the conductivity to roughly 1 $\mho$/m [3,4], a 20-fold increase. However, the vehicle-scaled power requirement of an air-breathing engine incorporating thermal ionization and thrust generation by an electromagnetic accelerator currently may only be met by a system such as an on-board nuclear reactor. Research in this field waned by 1970.

For control surface aerodynamics, thermal ionization, whether augmented by seeding or not, may not be feasible or even desirable. Its benefits and drawbacks have been discussed for concepts like the MARIAH hypersonic wind tunnel facility [5] and the AJAX scramjet power generator [6–8]. In particular, seeding may contaminate the flow of the MARIAH wind tunnel. At speeds below that which result in significant shock-induced ionization, EMFC may have serious limitations compared to its overall benefits since a separate non-thermal ionization system must be utilized. A few situations do exist in which ionization is currently experienced by an aerospace vehicle. For instance, the Space Shuttle interacts with ionized particles while in low Earth orbit [9] and during re-entry, where the re-entry environment has resulted in numerous studies (e.g., Refs. [10,11]) of how to improve current vehicle designs with the addition of electromagnetic fields. However, with the Space Shuttle's impending retirement and no new prospects for the incorporation of actuators into full-scale space vehicles (assuming the Orion design is nearly finalized), less grandiose platforms like hypersonic missiles may currently be the best near-term candidate for EMFC systems. With that in mind, the flight Mach number may be limited to below about 15, for which artificial creation of an adequate amount of flow conductivity is necessary. Recently, generation of a conductive gas, also known as a weakly ionized gas (WIG), has been accomplished using high voltage fields, laser beams, or perhaps directed microwaves [12,13]. However, these ionization methods produce a far lower level of conductivity when compared with results from 50 years ago. Experimentally, the maximum realized values of σ in air are currently in the $0.1-1\,\mho$/m range with high voltage fields. Raising the gas conductivity and minimizing power consumption are obviously priorities if practical aerospace systems are to be realized.

Also of significant note has been the development of flow control systems utilizing only an electric field to create plasma. The design of an EFC device with only a high voltage field is much less complex since the field will ionize the air itself. Electrohydrodynamic flow control techniques can be divided into two categories: glow discharges and dielectric barrier discharges (DBDs). The physics for the two categories is similar. An air gap

exists between the anode and cathode region of a glow discharge, while a much thinner dielectric material barrier is used for DBD systems which limits arcing. Paschen's law states that the electrical breakdown voltage is based on gap distance and pressure. Because the anode and cathode of a DBD are separated by a thin dielectric gap, the operating pressure is higher and additionally the high electric field significantly raises the output Coulomb body force. Because of a larger air gap distance, most glow discharge research has occurred with low pressure and the control mechanism is thought to be more of a thermal effect. Although both systems solve the conductivity generation problem by ionizing the air without a separate system, the value of σ is very low, even $10^{-5}-10^{-7}$ $\mho$/m for some DBD actuators. Both systems also operate often using low power requirements that may be met by current on-board generators.

One may assume the magnitude of the force generated by electric or electromagnetic fields is naturally a reflection of the amount of power consumed. Considering the potential use of each in the aerospace industry, there is a tendency to associate electromagnetic fields with systems consuming a large amount of power. Systems based solely on the Coulomb force have been proposed and used for applications with relatively less power (i.e., electrostatic ion thrusters and ion lifters). Therefore, a fundamental issue to address for the future of flow control using these fields is defining how much power is needed for an appreciable control force. Put another way, while an electromagnetic field is generally associated with larger scale aerospace applications and may be more robust, an electric field may be all that is necessary to generate a satisfactory control force. The answer to this question will likely cause one to eventually be far more appropriate for use over the other.

Recent experimental results have not entirely addressed this issue, although some progress has been made. Aerospace research involving electromagnetic fields has focused on hypersonic flows [14], particularly for the augmentation of scramjet propulsion systems. Most work involving MHD and scramjets has been computational, which is clearly understandable due to the cost and complexity of testing. However, this situation has led to significant differences between experimental and computational work. Experimental values of pressure, conductivity and magnetic field strength are usually below what is assumed analytically or in computational simulations. For example, Bruno et al. assumed a magnetic field between 7 and 17 T as part of a first-order electromagnetic hypersonic propulsion system [15]. In another design, Park et al. computed values of $B = 11.28$ T, $\sigma = 35.87$ $\mho$/m (with seeding) and $p = 1.25$ MPa at the entrance to the scramjet's MHD accelerator [16]. Recent experimental environments have been generally limited to 0.5–4.0 T, at most a few $\mho$/m, and rarefield pressures. Low pressure testing has been a method to increase I_M understandably as such conditions facilitate ionization. Little discussion has been articulated on the subject matter of selecting appropriate values of these parameters for aerodynamic control surfaces. Interestingly, these experimental values of B, σ and p might be better suited for control surfaces rather than for propulsion systems. Practical values of crucial scaling parameters must be established so as to define what value ranges should be associated with larger, propulsion-associated systems and smaller control surface systems.

Conversely, electrohydrodynamic flow control surfaces have mostly been experimentally demonstrated with low freestream speeds and Reynolds numbers [17]. These demonstrations represent a significant departure from the high-speed flight regime where electric and electromagnetic fields were first considered for use. This situation is especially true for DBDs. High-speed experimentation has appeared with glow discharges, but the studies have historically centered upon bluff bodies more than aerodynamic surfaces. Again, static pressure is often in the range of a few torr to facilitate the creation of a diffuse electrical discharge. Although the high-speed control effect of glow discharges appears to depend more on an increase in of the local speed of sound caused by Joule heating rather than the presence of an electrohydrodynamic force, rapid control actuation is desirable. Increasing the Reynolds number while still providing effective control with these systems is crucial. For flow environments besides very low speeds where DBDs appear best suited, glow discharge and EMFC concepts are competitive for a wide range of control possibilities.

2. Magnetohydrodynamic interaction and scaling

The central difference between electrohydrodynamics (EHD) and magnetohydrodynamics (MHD) is the force produced during the interaction of ionized particles with the electric or electromagnetic fields, respectively. For EHD, it is the Coulomb force while for MHD it is the Lorentz force. These interactions are often summed up in one equation written as

$$\mathbf{F} = q(\mathbf{E} + \mathbf{u} \times \mathbf{B}). \tag{1}$$

With research in electric and EMFC beginning to focus mainly within the boundary layer where E is high and u is low, there is a tendency to observe Eq. (1) and conclude that the presence of a magnetic field has little effect on the magnitude of the body force from a simple order-of-magnitude comparison of the two terms on the right-hand side. This conclusion is incorrect since both RHS terms of Eq. (1) actually contain an electric field component. Note that the $u \times B$ product is actually an electric field, usually referred to as the internal-induced electric field in channel flow applications. The single E term is referred to as the applied or external electric field for accelerators and generators, respectively. Interaction of only an electric field with ionized particles will produce a body force, but its relative magnitude with respect to the force produced by an electromagnetic field cannot easily be determined by Eq. (1). A strong current field interacting with ionized particles can create an induced magnetic field, but that field and any body force generated from that interaction is likely negligible for EMFC as will be shown. The concepts above have been well established in the literature [18,19].

In order to provide insight to MHD interaction and scaling, a derivation of the EHD and MHD forces is useful. Coulomb's law states that two charged particles exert a mutual force in a direction parallel to the line connecting each particle. If one of these particles is held stationary in the reference frame of the other one, it creates an electric field and exerts a force on the other particle, written as

$$\mathbf{F}_2(\mathbf{r}_2) = eZ_2\left[\frac{eZ_1\ (\mathbf{r}_2 - \mathbf{r}_1)}{4\pi\varepsilon_0|\mathbf{r}_2 - \mathbf{r}_1|^3}\right], \tag{2}$$

where the bracketed term represent the electric field. Similarly, the magnetic force law states that a force is developed between two current carrying wires which is dependent on distance and, additionally, the orientation of the wires. Over a length of wire **dl** this force is written as

$$\mathbf{dF}(\mathbf{r}) = \frac{\mu_0}{4\pi}\frac{II'}{|\mathbf{r} - \mathbf{r}'|^3}\mathbf{dl} \times [\mathbf{dl}' \times (\mathbf{r} - \mathbf{r}')], \tag{3}$$

where the prime is used to denote the properties of one wire from another. Invoking the Biot–Savart law leads to an expression for the magnetic field at r, namely,

$$\mathbf{B}(\mathbf{r}) = \frac{\mu_0}{4\pi}\int_{l'}\frac{I'(\mathbf{r}')\,\mathbf{dl}' \times (\mathbf{r} - \mathbf{r}')}{|\mathbf{r} - \mathbf{r}'|^3}. \tag{4}$$

Next, using Ampere's law, Eq. (3) can be simplified to

$$\mathbf{dF}(\mathbf{r}) = I(\mathbf{r})\,\mathbf{dl}(\mathbf{r}) \times \mathbf{B}. \tag{5}$$

If S denotes the cross-sectional area of the wire, n denotes the number of particles and the subscript p denotes a particle along the wire, then the force is

$$\mathbf{dF} = n_p e Z_p S\,\mathrm{d}l\,\mathbf{u}_p \times \mathbf{B}. \tag{6}$$

Furthermore, the force on one particle is

$$\mathbf{F}_p = eZ_p\mathbf{u}_p \times \mathbf{B}. \tag{7}$$

Therefore, the combined electric and magnetic forces on a particle are

$$\mathbf{F}_p = eZ_p(\mathbf{E} + \mathbf{u}_p \times \mathbf{B}). \tag{8}$$

Neglecting polarization and magnetization effects, the body force components on an ionized gas or liquid are shown in Eq. (9), which also has omitted the Hall effect (which can be significant) and ion slip:

$$\mathbf{F} = \rho_e\mathbf{E} + \mathbf{J} \times \mathbf{B}. \tag{9}$$

Next, the order of magnitude of these electric and electromagnetic Lorentz force components can be approximated, allowing for a comparison between the two [18]

$$\rho_e E \approx \frac{\varepsilon_0 E^2}{L}, \tag{10}$$

$$F_L = |\mathbf{J} \times \mathbf{B}| \approx \sigma(E + uB)B. \tag{11}$$

The relative magnitude of the two terms approximating F_L in Eq. (11) is critical for EMFC characterization. From Eqs. (10) and (11), the ratio of the electrohydrodynamic force to the magnetohydrodynamic force is

$$\frac{F_{EHD}}{F_{MHD}} = \frac{\rho_e E}{|\mathbf{J} \times \mathbf{B}|} = \frac{\varepsilon_0 E^2}{\sigma L(E + uB)B}. \tag{12}$$

With the potential difference between electrodes on MHD accelerators and recent EMFC actuators usually on the order of 1000 V or less, it is apparent that the electrohydrodynamic force will be negligible, unless the characteristic length is very small. Aerodynamic control systems will operate in far larger environments.

For EMFC characterization, it appears that much progress is needed to support experimental research. Historically, the magnetic interaction parameter I_M has been used to define the ratio of magnetic body force to the inertia of the fluid:

$$I_M = \frac{\text{EM forces}}{\text{Inertia forces}} = \frac{\sigma B^2 L}{\rho u}. \tag{13}$$

The prospects of reaching $I_M \approx 1$ were discussed as a performance benchmark in literature decades ago (e.g., Ref. [20]) and has seen use again with many recent EMFC publications. However, these recent EMFC environments usually demonstrate $I_M \ll 1$ and it takes a combination of very high flow speed and low density to reach unity. Despite having a low value, these same experimental results still demonstrate appreciable changes to the flow. As Elsasser remarked, dimensional relations in MHD are often much larger or much smaller than unity [21]. Perhaps other dimensionless numbers are more suitable for characterizing and scaling the effects of EMFC. With pressure changes often measured to confirm the effect of the Lorentz force, variables to consider include B, E, ρ, p, u, L, and σ. Table 1 shows several resulting dimensionless numbers derived using the Buckingham Pi theorem.

The most common term developed from Table 1 is E/Bu, referred to as the MHD loading parameter. It can be seen as a ratio of the total power per unit volume added to the flow to the directed kinetic energy [2]. As such, the parameter should be minimized to raise the conversion efficiency of energy used to accelerate the flow (rather than letting it contribute to Joule heating). From the last combination of variables, E/Bu and I_M are formed. As is common with Buckingham Pi theorem results, two dimensionless numbers can be multiplied to form further dimensionless parameters. Usually only a few will have significance, and one to highlight from that set is distinguished as the electromagnetic interaction parameter:

Table 1
Resulting dimensionless numbers for several EMFC variable combinations.

Variable combinations	Dimensionless numbers
B, E, σ, u, p	$\frac{E}{Bu}$
B, E, σ, u, ρ	$\frac{E}{Bu}$
B, E, σ, L, p	$\frac{BE\sigma L}{p}$
B, E, σ, L, ρ	$\frac{B^3\sigma L}{E\rho}$
B, E, σ, L, p, u	$\frac{E}{Bu}; \frac{BE\sigma L}{p}$
B, E, σ, L, ρ, u	$\frac{E}{Bu}; \frac{\sigma B^2 L}{\rho u} \rightarrow \frac{BE\sigma L}{\rho u^2}$

$$I_{EM} = \frac{BE\sigma L}{\rho u^2}. \tag{14}$$

This parameter, like I_M, is a ratio of the magnetic body force to the fluid inertia. It is interesting to note their individual similarity to one of the respective Lorentz force components shown in Eq. (11). Although $E \approx Bu$ has been assumed in the derivations of many publications (e.g., Refs. [18,21]), this assumption is not necessarily valid for small-scale environments like boundary layer EMFC where E is high and u is low. In fact, it appears that I_{EM} and I_M are useful over separate design spaces depending on where $E \gg uB$ or $E \ll uB$, respectively. The term $B^3\sigma L/\rho E$ has not seen use, and is another product of the MHD loading factor and the interaction parameter. The term developed in the third row is interesting since it relates a magnetic force to static pressure, which may prove to be useful with further experimental testing. Another modified interaction parameter that has appeared in the literature is [12,22–24]

$$I_{BL} = \frac{\sigma B^2 L}{\rho u_\infty \sqrt{c_f/2}}. \tag{15}$$

This term defines u as the friction velocity, whereby $u^+ = u_\infty\sqrt{c_f/2}$. As research into boundary layer EMFC increases, this term and velocity profiles using the inner-law variables should be useful in comparing effects over different test facilities.

As an example of the importance of these parameters, consider a flat plate, EMFC actuator with five surface electrodes each separated by 1.59 cm of dielectric material as shown in Fig. 1. The electrodes alternate with embedded magnets. The figure is a computer rendition of an actuator constructed and tested [25], with the dielectric material shown as transparent. Such actuator geometry may be typical for surface EMFC as the field progresses. Flat plate actuators with alternating magnets and electrodes have been previously demonstrated with salt water environments as can be seen in [22] along with a discussion of related research. The middle and outer electrodes are grounded, while the potential of the other two is 500 V. The length and width of the electrodes are 1.27 and 0.51 cm, respectively. The permanent, NdFeB magnets, 1.27 cm square by 2.54 cm long, are embedded about 1 mm below the surface. The measured magnetic field across the surface of the actuator B is shown in Fig. 2. Next, assume this device is operating under a freestream airflow of 1000 m/s. The conductivity of the air

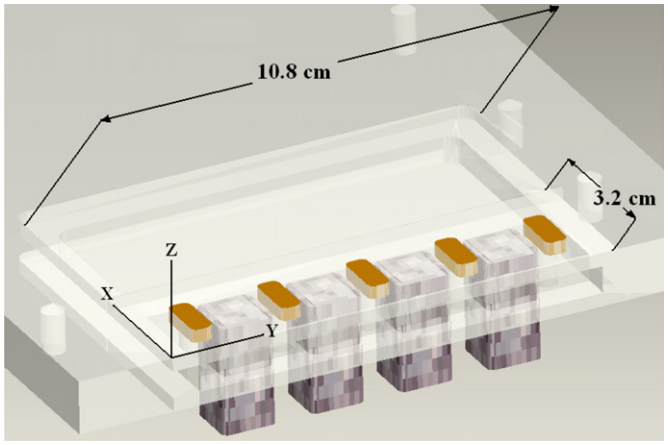

Fig. 1. Image of the five electrode, four magnet actuator plate with dielectric material shown as transparent.

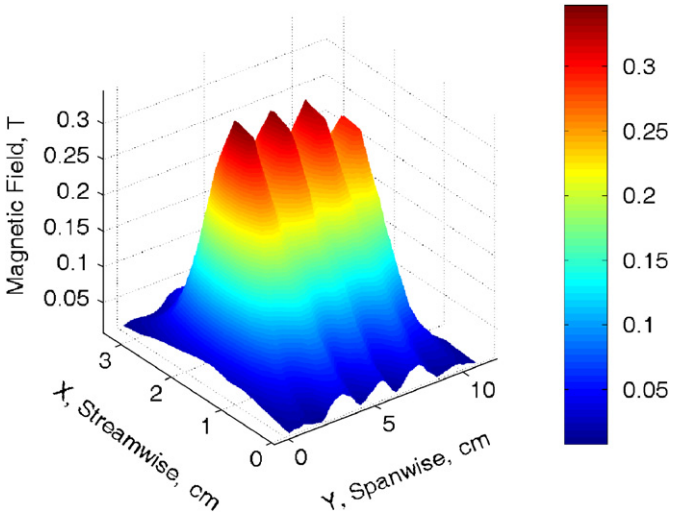

Fig. 2. Total magnetic field located on the surface of the flat plate over the 10.8×3.2 cm area.

is arbitrarily set to be $1\,\mho$/m, produced by a separate ionization system. The boundary layer thickness has been fixed at 1.0 cm and the velocity profile follows a typical turbulent shape. The boundary layer velocity as a function of height off of the flat plate is denoted as $u_{BL} = u(z)$.

The magnetic field components (B_x and B_y), actuator geometry, and electrode potentials were used as boundary conditions in a computational MHD code to determine the Lorentz force and interaction parameters. The magnetic field generated showed reasonable agreement with experimental magnetic field measurements that were taken up to $z = 1.27$ cm.

Fig. 3 shows the common logarithm of the local Lorentz force for a two-dimensional spanwise slice over the actuator at $x = 1.8$ cm. The locations of the magnets and electrodes are labeled at the bottom. The Lorentz force is most heavily concentrated over the electrodes and especially at their edges where electric charge builds. The magnitude of the Lorentz force produced in part with the NdFeB magnets drops significantly with height, but remains viable for boundary layer applications. The Lorentz force is not as high over the outer electrodes because they are grounded. In this spanwise arrangement, it is important to keep the outer electrodes grounded to prevent a counteracting body force from developing past the edges of the actuator.

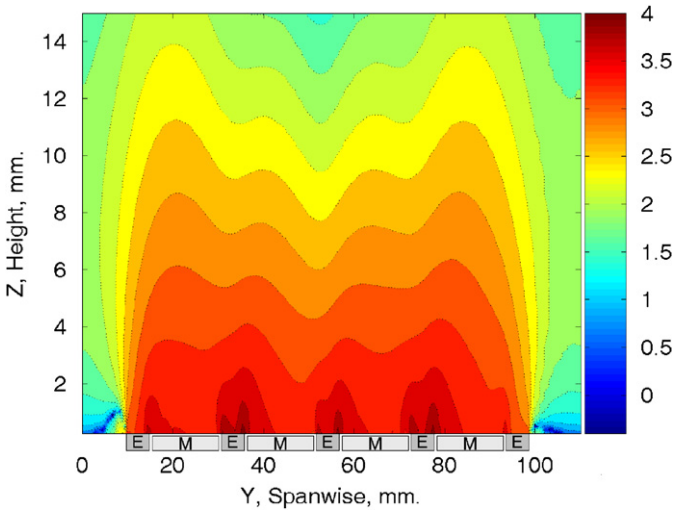

Fig. 3. The common logarithm of the Lorentz force (N/m^2) across a spanwise slice over the actuator at $x = 1.8$ cm.

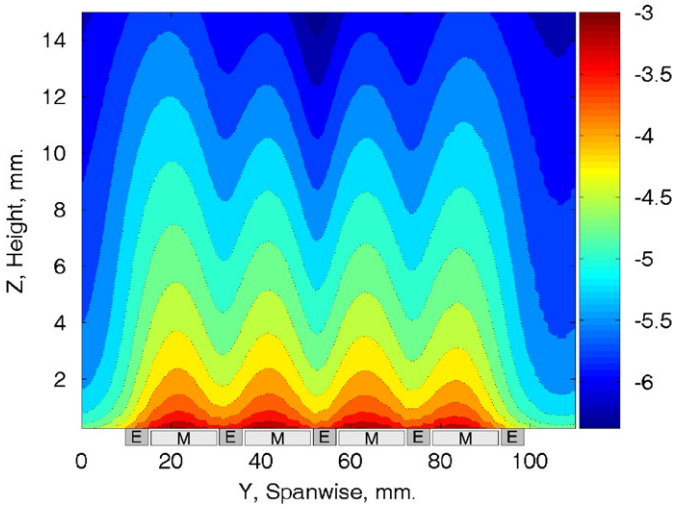

Fig. 4. The common logarithm of I_M/L across a spanwise slice over the actuator at $x = 1.8$ cm.

Figs. 4 and 5 show the common logarithm of the local interaction parameters I_M and I_{EM}, respectively. Logarithms are used for two reasons, first, because the localized values range over several orders of magnitude. Second, the similarities and differences between the figures are more important than the actual values. For the calculation of the parameters, ρ was approximated as $1\,kg/m^3$ throughout the boundary layer. (In actuality it will increase or decrease towards the surface depending on the wall conditions.) Additionally, L was removed from the parameters since it is not meaningful for the two-dimensional slice of interest. Fig. 4, as would be expected, shows I_M distinctly centered upon the embedded NdFeB magnets. If I_M is truly a good choice as a non-dimensional representation of the Lorentz force for this actuator, then the localized contours of Figs. 3 and 4 would be similar. An evaluation of the data used for this example indeed shows that $E \gg uB$ across the boundary layer. Fig. 5 shows that the Lorentz force more appropriately follows the same contours as I_{EM}. In Fig. 5, the maximum values of I_{EM} are centered on the electrodes. The only difference between the figures is I_{EM} is more uniform near to the actuator surface because of the use of u_{BL}^2.

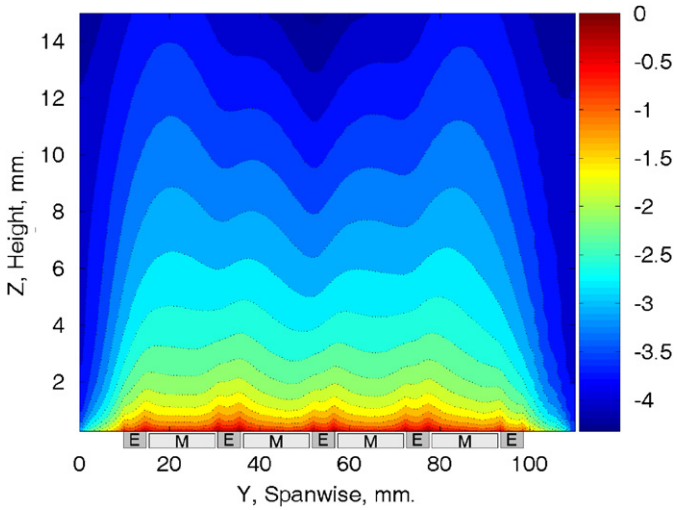

Fig. 5. The common logarithm of I_{EM}/L across a spanwise slice over the actuator at $x = 1.8$ cm.

The consequences of selecting the correct interaction parameter for an actuator will have a larger impact than the comparison of these figures. Most important, the performance will scale differently with E, B, and u depending on the value of the MHD loading parameter. On a case-by-case basis, the average of the localized MHD loading parameter in the boundary layer should be known before the actuator and its operating conditions are characterized by I_M or I_{EM}. Although I_M has been more widely used than I_{EM}, the example shows that the design space over which I_{EM} is applicable is significant. Also, where $E \approx Bu$, neither term may be appropriate for correctly scaling the Lorentz force effects.

Going back to Fig. 3, the Lorentz force is noticeably non-uniform across the span of the actuator. This may be unavoidable for surface actuators since the electric and magnetic fields have inherently large gradients. The simplest strategy for creating some uniformity is to match the maximum B field points with the minimum E field points and vice versa along the actuator surface. Earlier MHD studies have shown that the geometry of segmented electrodes has a large impact on the distribution of the electric field [26], and that observation certainly applies to this example actuator. As the MHD loading parameter decreases, the maximum Lorentz force locations will gradually shift from over the surface of the electrodes to over the magnetic poles.

Computing these local parameters is only practical in a computational environment, but doing so may be necessary before accurately scaling the performance of the actuator with any particular interaction parameter. Establishing u as the friction velocity in the manner of I_{BL} for comparison purposes across different facilities is recommended.

Continuing on, the magnetic Reynolds number is a measure of the ease with which an ionized gas moves through a magnetic field, and is defined as

$$Re_M = \mu_0 \sigma u L. \tag{16}$$

The number can also be seen as a ratio between convection and magnetic diffusion effects, where diffusion (and therefore B) dominates the system for $Re_M \ll 1$ [27]. When $Re_M > 1$, the motion of charged particles in a current field can create an induced magnetic field b, responsible for many astrophysical phenomena. A relationship between the magnetic Reynolds number, the current field, and the induced magnetic field is

$$Re_M \mathbf{J} = \nabla \times \mathbf{b}. \tag{17}$$

With the aforementioned ranges of σ, u, and L, the magnetic Reynolds number is far lower than unity within the boundary layer for this example actuator. This result should be true for most if not all EMFC actuators, as the creation of an induced magnetic field for a flight vehicle needs a combination of very high speed and a current field likely too large to be supplied by an on-board generator.

3. EMFC surface actuator design issues

For electromagnetic fields to be successfully applied into a control surface actuator, several issues must be considered. First, while channel flow setups are ideal for understanding the physics of EMFC, open flow experiments must be considered in which the EMFC actuator is contained in a flat plate or airfoil. Power consumption and packaging are important issues to address, with the selection of magnets and the method of ionization key to success. The selection of EMFC magnets is a significant matter since rare-earth materials would be ideal for placement inside a thin control surface, except for the major problem in which their field strength is relatively low and adversely affected by heat. Finally, unlike EFC, a sufficiently high value of conductivity must be created by an additional system for applications in which thermal ionization is not encountered in the flight regime chosen.

3.1. Channel flow and open flow experimentation

While one of the focal points of EFC has been for control surfaces, the same cannot necessarily be said for EMFC systems thus far. EMFC experiments applied to aerospace systems have typically been for scramjet-like systems and have taken place in a channel flow environment. Analytical approaches have also been well established for MHD channel flows while open flow modeling requires more sophistication. The design highlights and operating conditions of several recent facilities are discussed below. Ionization systems for each facility will be elaborated upon further into the text.

One recent channel flow facility has been developed with the intent to place an accelerating or retarding Lorentz force on a high-speed flow (Mach 3–4) of air or another mixture of gases [12,23,28–37]. The walls of the test section each have electrodes mounted into them. Two electrodes mounted opposite of each other create a WIG in the test section using high voltage, low duty cycle pulsing while the other two are connected to a DC current system. That system provides the energy for the Lorentz force so long as the level of conductivity provided by the ionization electrodes is enough for current to cross the electrode gap. The Lorentz force may be applied with or against the flow depending on the electrode and magnet polarity. Experimental data collected have included flow visualization, flow fluctuation measurements, Lorentz force-induced pressure changes, and the output of the ionization and Lorentz force systems.

The test section static pressure of this facility ranges from 5 to 20 torr. The channel itself is small enough to be surrounded with an electromagnet that can reach $B = 2$ T, while a NdFeB magnet configuration ($B \approx 0.4$ T) was also demonstrated in earlier works [12,30]. A decrease was measured in the pressure fluctuation due to the Lorentz force in Ref. [12], but no direct measurements of pressure were taken at the time. The flow conductivity from the ionization system has risen with more recent publications, and is usually on the order of 0.1 $\mho$/m. Further studies with electromagnets have shown large pressure differences created by the Lorentz force. For instance, Nishihara et al. [29] have shown a static pressure increase of 17–20% for a retarding force and 5–7% for an accelerating force of the same magnitude. Similar data of

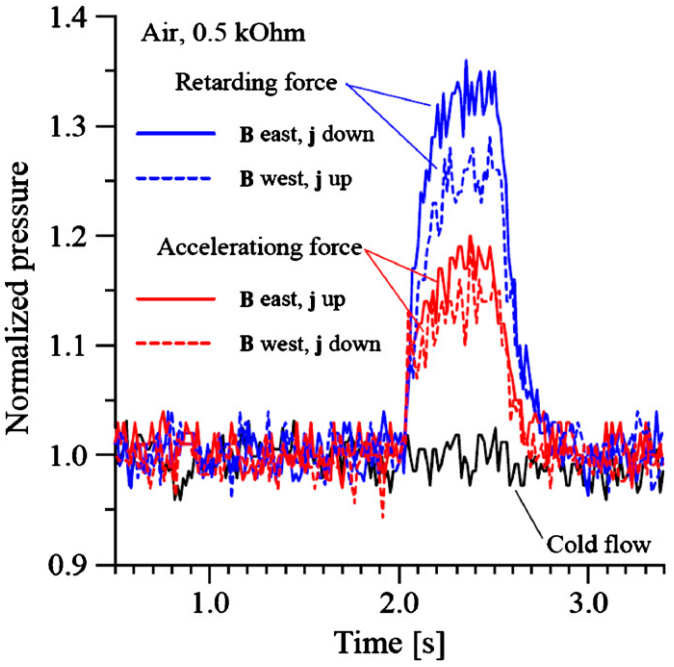

Fig. 6. Normalized static pressure traces downstream of an EMFC actuator for $M = 3$ dry air for four electromagnetic arrangements (from [35]).

greater magnitude from [35] are shown in Fig. 6. The figure shows the normalized pressure difference for dry air between unaltered flow, flow with a retarding force, and flow with an accelerating force. The retarding force is more effective than the accelerating force because it works with Joule heating to create the rise in pressure, while the accelerating force works against Joule heating. The magnitude of the pressure rise also appears to be dependent upon Lorentz force polarity, where it is suggested that the test section Mach number and pressure are affected by the electromagnetic force interaction.

Another channel flow test section has been constructed to explore the effects of a constricted plasma column operating under the presence of a magnetic field [38]. In the test section, two tapered electrodes were placed on the side of one of the tunnel walls. After actuating a high voltage DC circuit, a constricted plasma column forms between the electrodes and propagates downstream due to the tapering. A helium-cooled superconducting ring magnet surrounds the channel and can generate a B field up to 7 T, which increases the velocity at which the plasma column travels [39]. Since EFC systems are based on momentum transfer due to collisions between the ions and a neutral flow, this system can be seen as a novel method to enhance the momentum transfer using magnetic fields. Instead of two separate power supplies for ionization and Lorentz force generation, a single 20 kV, current regulated power supply is used. The electric field generated by the 20 kV potential ionizes the gas to the point of breakdown, and the resulting arc draws up to a specified current limit. Once the current limit is reached, the power supply voltage drops significantly, so the power input into the flow is considerably less than its maximum value of 20 kW. Therefore, the initial 20 kV potential before breakdown acts like an ignition system for the EMFC actuator.

The test section has a Mach number of 2.8 and static pressure of 28 torr. Experimental data collected consisted of static pressure measurements in addition to flow visualization. A wedge was placed inside the test section to study the effects of the system on shock/boundary layer interaction [39]. Results show that the actuator is able to move the separation bubble induced by the shock interaction, and the static pressure across the wedge is affected.

A third facility has been developed with a flat plate secured inside a free jet test section designed for basic research in MHD [40]. An electromagnet with a maximum field of 3.5 T surrounds the entire channel, and a NdFeB configuration has also been tested. The Mach number in this facility is about 5.0, and the test section static pressure is designed to simulate an altitude between 30 and 50 km (approximately 0.6–7 torr). Besides covering the altitude range mentioned, the low test section pressure has also been designed with consideration to raising the value of I_M, which reaches approximately 1.5 per meter. The flat plate, shown in Fig. 13, has two embedded electrodes which use high voltage DC, RF, or a combination of both fields to ionize the air up to 2.5 $\mho$/m. The figure also shows the rarefied air pressure in the test section allows for a relatively low voltage glow discharge to transmit a substantial amount of power to support the Lorentz force.

Before incorporating a flat plate into the facility, tests were conducted with blunt body configurations at Mach 5.8 where experimental results included plasma diagnostics and aerodynamic force measurement [41]. For the flat plate configuration, surface pressure measurements indicated that a Lorentz force directed out of the plate has more of an effect than directing it into the plate, again due to flow coupling and Joule heating issues [42]. Both push the luminous region of the glow discharge onto or off the actuator surface. Although a glow discharge raised lift by up to 18% in one set of experiments, applying a magnetic field can negatively affect the discharge and void the change in lift [43]. A more recent study has moved to testing rectangular and cylindrical inlets supported by computational modeling [44].

EMFC publications have increased in the past few years and other facilities are likely to join those above. The ionization systems and overall electrode design for the generation of a WIG or plasma column and interaction with a magnetic field to produce the Lorentz force appear to be feasible for high-speed, boundary layer EMFC based on results from these facilities. However, the value of conductivity generated (0.1−2.5 $\mho$/m) by the high-voltage systems as well as the test section pressure are several orders of magnitude below those that may be necessary for the AJAX engine concept. It would be very interesting to modify the geometry and examine the performance of these facilities under an open flow, flat plate environment with pressures closer to what may be encountered by a wing or fin during high-speed flight. Magnets for such applications should also be embedded in the surface. Control of slender wings and fins, and perhaps the initial stage of an inlet compression system, are likely the best applications for these systems. If changing the geometry and increasing p are not formidable obstacles, perhaps these types of systems could be placed on a high-speed missile for control purposes.

With electromagnetic fields, experimental measurements can be difficult because of signal interference. Typically, one or more transducer ports are placed downstream of the electromagnetic arrangement to capture the change in static pressure resulting from the Lorentz force. These data, along with flow visualization, power input, and plasma diagnostics results provide the means to understand the basic physics of EMFC. The measurement of aerodynamic forces, conducted in a few studies, will need to become more widespread as the actuator designs become more representative of control surfaces. Since most EMFC studies have been primarily focused on boundary layer control, it is desirable to use more refined techniques to analyze changes to the boundary layer profile. The inherent non-uniformity of the Lorentz force field likely adds unusual effects that must be measured as a function of height above the plate as well as in the spanwise direction. Fig. 7 shows an example of the change in boundary layer

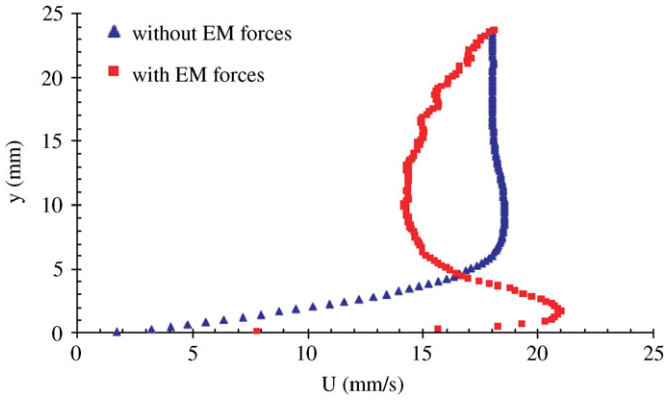

Fig. 7. Boundary layer velocity profile downstream of a flat plate EMFC actuator for salt water flow (from [45]).

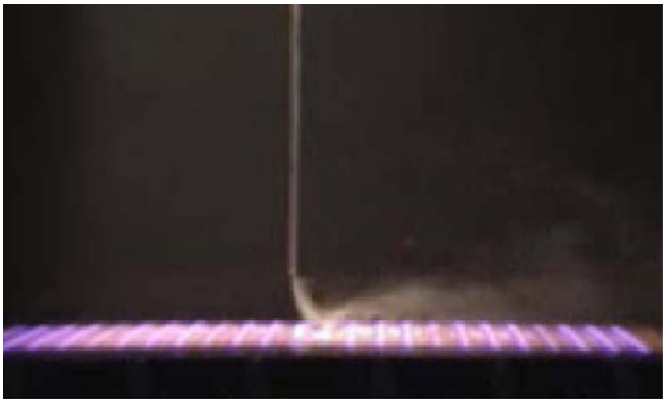

Fig. 8. Smoke visualization of a DBD control surface composed of rows of actuators creating an electrostatic force that acts from left to right (from [52]).

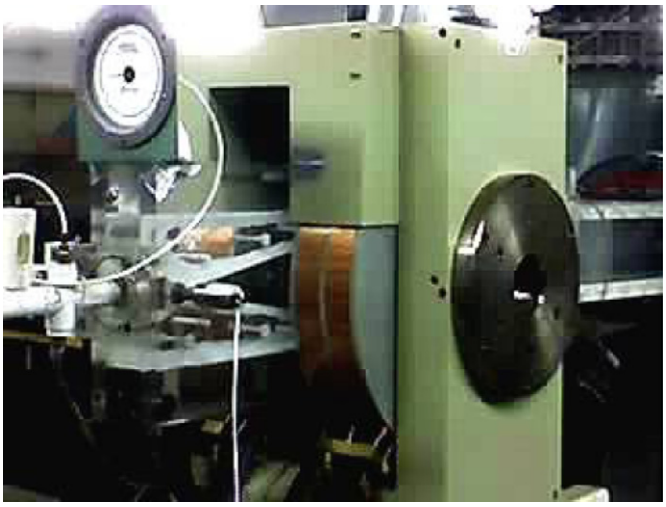

Fig. 9. A water-cooled electromagnet surrounds an EMFC free jet test section (from [43]).

profile for a low-speed salt water freestream flow of about 18 mm/s as measured with a particle image velocimetry (PIV) system. Since salt water is naturally conductive (a few $\mho$/m), flat plate Lorentz force actuators have been much easier to build, test, and characterize [22,45]. PIV imaging directly over an EMFC actuator for gas flow may be difficult because of the luminosity of the ionized gas and Lorentz force energy addition.

Although the flow speed in Fig. 7 is very low, other research with salt water has been conducted at higher speeds. The concept of EMFC and propulsion for naval applications has existed just as long as it has for aircraft [46]. The concept has also been proven with subscale submarines and ships [47,48]. A collection of papers in this field concerning electromagnetic drag reduction can be found in Ref. [49]. Studies of MHD propulsion have concluded that it is feasible and desirable because of stealth [50], but effects from bubble formation at the electrodes in salt water and the generation of hydrogen and chlorine gas will need mitigation. MHD propulsion for a full-scale submarine will require significant power and new developments in efficiency for on-board nuclear reactors.

3.2. *Power consumption and packaging*

For EFC systems, power consumption and packaging are relatively simple issues. Glow discharges require high voltage, but they are generally low power phenomena. DBDs also require high voltage, but the low operating current again leads to low power consumption. Corke and Post report a power level of approximately 6.5–130 W per spanwise linear meter for DBD actuators [51]. Fig. 8 shows the ease at which these DBD actuators can be placed onto a surface as long as the material they are embedded in is dielectric [52]. Since the actuators are thin in the streamwise direction, the power requirement is anywhere between several hundred watts and a few kilowatts per square meter of a hypothetical control surface built from placing them into rows. In the figure, the separation between DBD strips is 1.0 cm, and the RF signal input is 4.5 kV RMS at a frequency of 3.3 kHz. At these conditions, a flow speed of 6 m/s is induced at the edge of the panel. The thrust from these DBD arrangements rises with dissipated power [53]. Assuming the induced flow speed for flight-ready control surface actuators will need to be higher than a few meters per second, they will eventually have significantly higher power consumption than what was reported in Ref. [51].

Since glow discharge and DBD systems often use these thin sets of electrodes, packaging into control surfaces is also straightforward. The largest components of these systems may indeed be the high voltage circuit elements. As Jayaraman et al. discuss, increased interest in low Reynolds number aerodynamic control for micro air vehicles (MAVs) has brought the use of DBDs into consideration [54]. Although current computational and experimental research appears promising, scaling down to smaller, low-speed vehicles that fit into the useful design space for these actuators may pose a problem due to the mass and volume of high voltage circuit components. Studies on the integration of these components to small-scale aircraft appear limited and it is recommended that future research efforts cover this topic.

Concerning EMFC systems, the packaging issue is more complex and dependent not only on the power requirement but the choice of magnets. Fig. 9 shows a large electromagnet surrounding a hypersonic test section. As used in Ref. [43], it generated a magnetic field of 0.9 T. Although electromagnets used for experimental channel flow EMFC are useful in that they can provide a steady magnetic field inside the test section (whereas a field from NdFeB magnets will vary as shown in Fig. 2), their ability to be integrated into flight vehicles is questionable due to their mass and weight. The use of superconducting magnets only exacerbates the problem. The use of rare-earth magnets will lead to the most compact EMFC actuator that may be placed on the surface of a wing or at the beginning of an inlet compression system. Clearly, the drawback of efficient packaging with embedded permanent magnets is the relative reduction in magnetic field strength across the control surface. However, going back to the discussion of the interaction parameters, if the

actuator performance is not wholly dependent on B^2, a reduction in B is easier to offset with one of the other variables.

Assuming EMFC surfaces themselves can be made compact enough for flight, there is still a problem with the possibility that the Lorentz force power requirements will exceed the output of a reasonable on-board generator. As discussed, ionization systems may also require a separate power supply. Lorentz force power requirement estimates similar to the one presented above for DBD actuators is still relatively unknown. The pressure increase of 17–20% in Ref. [29] was created with about 2 kW of power where the electrodes enclosed a volume of approximately 40 cm^3. This figure does not appear unreasonably high as many aerospace systems currently require power of that scale. The power supply requirements are also heavily based upon the time of use of the actuator. If the purpose is long-term drag reduction or lift enhancement, an innovative generator is probably required. Perhaps a short duration missile (with EMFC actuators for final, rapid course corrections) can operate based off a thermal battery typical of current technology. The fact that many other potential sources (MEMS microturbine generators, fuel cells, flywheels, capacitors, etc.) of compact on-board power supplies are under development is encouraging [55].

3.3. Selection of EMFC magnets

Concerning the viability of EMFC, an inquiry must be made to understand exactly what range of magnetic surface field values is needed. This inquiry leads back to the reason why magnets are needed for EMFC in the first place, namely, that the cross product of magnetic field and the electric field produces the Lorentz force. The presence of a magnetic field acts as a facilitator for energy addition into the fluid flow from the electrodes. The energy addition is then split into Joule heating and the kinetic energy (rate of work done by the Lorentz force) of the fluid. The selection of appropriate magnets for EMFC systems is a current topic of debate. As was mentioned previously, many recent experimental EMFC facilities have used powerful electromagnets capable of surrounding a test section since it is a straightforward way to increase the magnetic interaction parameter. However, some of these electromagnets and superconducting magnets have masses up to hundreds of kilograms (e.g., Ref. [39]) which will make flight applications problematic.

The advancements in several new rare-earth magnetic alloys between 1970 and 2000 [56] have made permanent magnets a competitive choice for aerospace applications of MHD. Preliminary demonstrations of their capabilities have been seen in several publications [12,22,25,30,40,45]. Permanent magnets, where possible, should be considered instead of electromagnets since they consume no power and demonstrate much higher values of energy density making their strength-to-weight ratio relatively superior. Unfortunately, one major drawback of using permanent magnets for aerospace applications is the fact that high temperatures drastically weaken their overall surface field strength, which is already low when compared to electromagnets. Permanent magnets lose their magnetic properties at a specified point called the Curie temperature. Prior to that point there is another temperature called the maximum operating point, after which a magnet will experience permanent losses to its original strength [57]. For AJAX-style scramjet engines, it is unlikely that permanent magnets could be used in the high-temperature environments even with robust active cooling systems.

Fig. 10 shows the maximum operational temperatures of samarium–cobalt and neodymium magnets charted along with typical post-shock temperature curves as a function of Mach number for different wedge angles with an incoming stream at

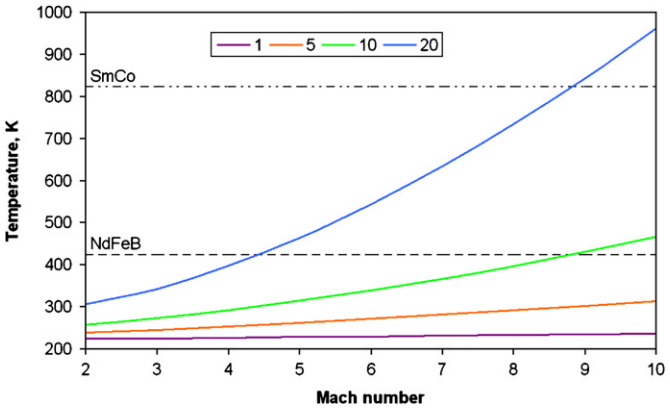

Fig. 10. Temperature versus Mach number for lines of constant wedge angle (1°, 5°, 10°, 20°) after an oblique shock wave (based on an initial temperature of 220 K) along with neodymium and samarium–cobalt maximum operating temperatures.

220 K. Neodymium magnets are operationally limited to temperatures just over 400 K, while some samarium–cobalt alloys can be used at temperatures exceeding 800 K. While these temperatures are still far below the requirements of implementation into, for instance, a multi-shock scramjet inlet, these magnets could be used for slender control surfaces to some extent on supersonic and hypersonic vehicles. Moreover, while it would appear that samarium–cobalt alloys are superior to neodymium for high-speed aerodynamic control because of the higher operating point, Fig. 11 shows that the high-temperature alloys typically have less overall magnetic field strength [58]. Note that the magnetic flux density is measured using teslas, but the values from Fig. 11 are not representative of the maximum magnetic field (also measured in teslas) that will be present on the surface of the magnets. Neodymium and samarium–cobalt magnets are widely available, but they rarely demonstrate maximum surface fields over 0.5 T. Fig. 12 shows that it is common for permanent magnets to lose the bulk of their surface field before reaching their maximum operational temperatures [59]. Typically, these magnets will see a slight linear decline in surface field for a limited temperature range before reaching a point of rapid decline extending to the maximum service temperature. One of the focal points of current research in magnet development has been to broaden the temperature range in which only a slight linear decline is present, with significant improvements made to samarium–cobalt alloys [60–63] and apparently much less work carried out with neodymium alloys. Literally tens of thousands of other alloys have been tested to determine if they produce a stronger magnetic field, with no significant findings. Another method that has been used in an effort to improve rare-earth magnets is to use exchange-coupling to effectively combine the benefits of so-called hard and soft phases of different magnetic materials [64]. A hard magnetic phase resists permanent demagnetization (i.e., B field reduction by heating), and a soft phase exhibits a high level of magnetization. This concept has been experimentally proven to raise the energy product of rare-earth magnets where the phases are combined in nanoparticle assemblies [65]. One of the key issues to resolve in this field is uniform nanoparticle dispersions of the hard and soft phases.

As far as the surface field is concerned, one can conclude that neodymium magnets are the better choice for applications with temperatures ranging up to 350 K. However, the typical decline of the neodymium surface field strength as shown in Fig. 12 indicates that the performance of samarium–cobalt magnets becomes comparable for higher temperatures. It appears that many, if not all, high-speed aerodynamic control concepts involving permanent magnets will require active cooling. This

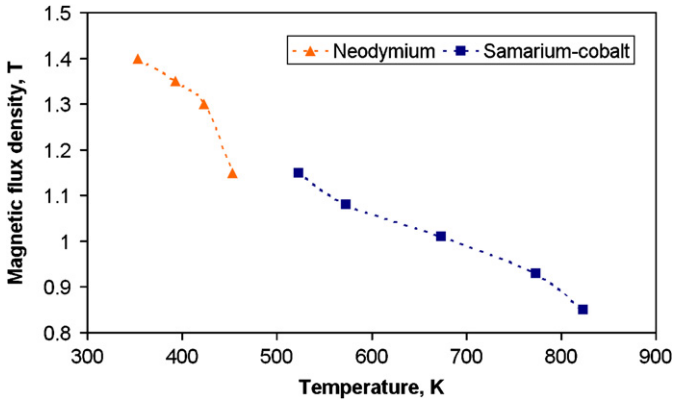

Fig. 11. Magnetic flux density charted as a function of the maximum operating temperature for several neodymium and samarium–cobalt alloys [58].

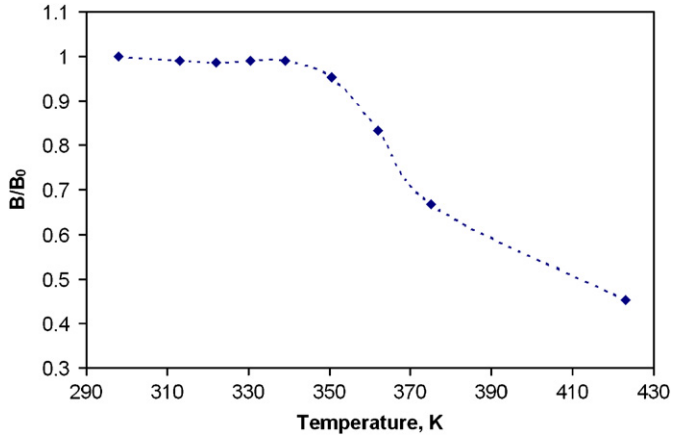

Fig. 12. A typical plot of the surface field decline versus temperature for a neodymium magnet with a maximum operating temperature of 423 K [59].

need for active cooling is not solely associated with the use of rare-earth magnets. As exemplified by Fig. 9, some electromagnets also require cooling just to operate.

3.4. Conductivity

In 1968, Garrison stated that the performance of MHD accelerators depends directly upon the magnitude of the electrical conductivity of the seeded working gas [66]. This statement remains true for aerodynamic control, only with more emphasis placed on improving low-temperature, WIGs. Before then, the concept of propulsion using electric and magnetic fields had appeared in the literature for several decades. Jahn presented a short review of early literature in electric propulsion [67]. Efforts at experimentation began in the late 1950s beginning with the implementation of plasma jets for propulsion systems [68]. Plasma jets were certainly capable of generating highly conductive gases through thermal ionization, but the temperature and power requirements were too high for viable aerospace applications at the time. Alkali salt seeding was introduced into the plasma jet in order to achieve the same level of conductivity at a considerably lower temperature [3]. Extensive experimentation with different low ionization energy seed materials (potassium and cesium) with air or noble gases (argon and helium) appeared in the literature through the end of the 1960s [69–77]. Generating a bulk flow conductivity on the order of 1000 $\mho$/m was achievable. The experimental gas pressures reported were usually on the order of one atmosphere. At higher pressures around 10 atmospheres, electron attachment by positive oxygen ions significantly reduces σ [78].

Like many other fields, research in MHD was affected by the direction of the Apollo program. It appears that engineers may have assumed that megawatts of power produced by an on-board nuclear reactor would be available for future MHD accelerator-based propulsion systems, but the nuclear prospect never materialized with the exception of the Project Pluto engine testing program [79]. Although nuclear-powered ramjet ground demonstrators were built and successfully tested during Project Pluto, the environmental concerns outweighed their strategic advantage. Additionally, the success of controlled ablation reduced the need for further research into EMFC for use on re-entry capsules [80]. Arc jets were then applied to ground testing systems with many integrated into wind tunnels as a source of high enthalpy, high velocity flow [6]. Seeding is still a viable method for increasing the performance of those wind tunnels, but it can lead to undesirable contamination of the flow. Simmons et al. concluded that discrepancies in the air chemistry caused by seeded MHD accelerator concepts for the MARIAH hypersonic wind tunnel made non-MHD options more appealing [81]. The lack of post-Apollo funding and interest in on-board nuclear power effectively halted the prospects of MHD systems for aerospace vehicles. Non-nuclear power generation became the new focus of MHD research [82,83]. Despite the fact that electric propulsion engines make use of a comparatively weaker force, concepts [84] developed simultaneously with those of MHD propulsion and eventually flourished with help of a low power requirement capable of matching with radioisotope thermo-electric generator technology then emerging [85].

The past decade has certainly seen a reemergence of MHD research applied to aerodynamics. The history above shows that generating and controlling a flow with $\sigma > 100\,\mho$/m is difficult because of the power requirements. Creating ionization from a thermal source such as a plasma jet is not desirable, and is not possible for aerodynamic control surfaces. Fortunately, ionization can also be achieved through high voltage fields, laser beams, microwaves, and radiation (any method of transferring energy to cause molecular excitation of the gas). Of the EMFC facilities mentioned thus far, all have at minimum employed high voltage fields. However, a difference exists between each on how the high voltage fields are applied.

The easiest method of creating plasma is to apply an electric field with a large potential difference between two electrodes. Based on factors like separation distance, potential difference, geometry, and the gap medium, plasma will develop between the electrodes. The current is based on the effective resistance of the gap. When plasma fills the gap, the resistance is immediately and significantly lowered. Normally, the end result is an arc discharge where the gap becomes a short circuit and draws maximum power from the potential source. Because of their difficulty to control and destructive nature, arc discharges are most often seen as detrimental for engineering applications. Thus for aerodynamic control, ionization with electric fields has focused on producing discharges of a more diffuse nature, known as glow or corona discharges. However, Zaidi et al. have in fact used a plasma column control concept operating in a constant current, variable voltage mode [38]. The power supply potential was 20 kVDC, and the maximum current was 1.0 A. Fixing the current and activating the power supply causes a high voltage field to be applied until electrical breakdown occurs and a plasma column forms. Once the column forms, the voltage required to maintain the set point current can be very low. When a plasma column forms between the path of least resistance where the tapered electrodes are closest to each other, it travels downstream where the gap

between the electrodes gradually increases, visually similar to a Jacob's ladder. The boundary layer control is provided by the momentum transfer from the plasma column propagating downstream.

During the wind tunnel experiments, the plasma column that forms between the electrodes was found to be periodic with a frequency of 1–10 kHz depending on the current and magnetic field strength [86]. While applying a 1.7 kV field at 35 mA with no magnetic field, the plasma column travels downstream at 360 m/s. When a magnetic field of $B = 2.0$ T is applied, the column speed increased to 2000 m/s [87] to generate the control results previously discussed. Thus the electric and magnetic fields combine to allow for greater momentum addition to the flow. It appears that the performance of this facility can be increased simply by raising the set point current. Unfortunately, Joule heating has worked against the plasma column in the case of moving a shock wave-induced separation bubble downstream and will begin to suppress results while current is increased beyond a certain point [39]. To conduct further studies with higher plasma column power, an assembly consisting of a sapphire base plate and high-temperature arc corrosion-resistant electrodes was constructed [87].

The DC ionization system first presented by Shang et al. [41] in 2002 was part of an EMFC actuator designed to affect the shock wave structure around a blunt body. A diffuse WIG is created instead of a plasma column due to a lower applied potential difference and a lower static pressure. The blunt body study was followed by a flat plate model constructed of a ceramic base and two embedded copper electrodes [42]. Fig. 13 shows these electrodes, with the upstream cathode experiencing a more intense glow [44]. This diffuse glow discharge begins to constrict and transition to an arc when the current surpasses 100 mA or when B is greater than 0.2 T [42]. In addition to using only a DC discharge, pulsing the discharge with a frequency between 5 Hz and 10 kHz was also used to explore the response of the Mach 5 flow to plasma actuation with a magnetic field present [88]. Volumetric heating of the air by the plasma was found to occur faster than the 3 ms response time of the pitot probe. In another case, RF radiation was added to augment the ionization created by the DC glow discharge, resulting in a reduction in the impedance across the electrode gap [40]. Accounting for all of the ionization methods, the maximum power requirement remained a few kilowatts or less and can result in a conductivity of a few $\mho$/m in the static pressure environment of 0.6–7 torr.

The research presented in the various publications for this facility certainly shows that a low-temperature WIG created by a DC discharge ionization system allows for energy addition in the boundary layer of high-speed air flow. As a result, the energy addition allows for an EMFC actuator to significantly affect the surface pressure distribution. Direct current discharges do not easily remain diffuse as pressure rises [89], but this system should be operational for high-altitude flight conditions.

Research has shown that the degree of ionization produced by an electric field may be higher for pulsed discharges rather than for a steady DC discharge of similar potential difference. Discharges with periodic high voltage pulses simply can withstand a higher applied electric field before a transition to arcing occurs, so long as they are sufficiently short enough to sustain streamers before transitioning to sparks [90]. This property allows more power to be transmitted during the pulse, which will increase σ. Very short duration, low duty cycle pulses can maintain a conductive path between electrodes as long as the frequency is additionally high enough to counteract the WIG decay. However, the applied Lorentz force should be continuous and therefore generated with a DC power supply. Palm et al. [12] addressed these issues by creating an EMFC channel flow facility with RF WIG generation and simultaneous DC Lorentz force application using the electrode configuration previously discussed. The facility generated a diffuse WIG for Mach 2–4 flow originally by using a 13.56 MHz, 600 W RF power supply to create the conductive path for the Lorentz force energy addition [30]. Conductivity ($0.1-1\,\mho$/m) scales with the power draw of the system. Since that time, a more complex ionization system has been constructed to raise the attainable level of conductivity without raising the power draw. Nishihara et al. reported using this system to attain $\sigma \approx 0.1\,\mho$/m in a Mach 3 flow by compressing a 500 V, 1 μs pulse into a high frequency (up to 50 kHz), high peak voltage (20 kV), short duration pulse (10–20 ns) [29]. During the peak voltage application, the current may reach 100 A, but the short duty cycle results in a reasonable overall power consumption of, for instance, 40–80 W in Ref. [29]. The ionization power requirement is therefore much less than what is used to apply the Lorentz force. According to Ref. [34], raising the frequency of the system from 40 to 50 kHz increases the flow conductivity along with lowering the ballast resistance. The frequencies in this range match reasonably well with the WIG decay and provide fairly steady flow conductivity.

The life of the WIG can be observed by measuring the current draw from the DC Lorentz force power supply. Fig. 14 shows four

Fig. 13. A DC voltage discharge between two electrodes at freestream conditions of $M = 5.15$ and $p = 0.59$ torr. The applied voltage is 880–920 V at a current of 50 mA. The addition of a magnetic field significantly affects the plasma and creates a virtual hypersonic leading edge strake (from [44]).

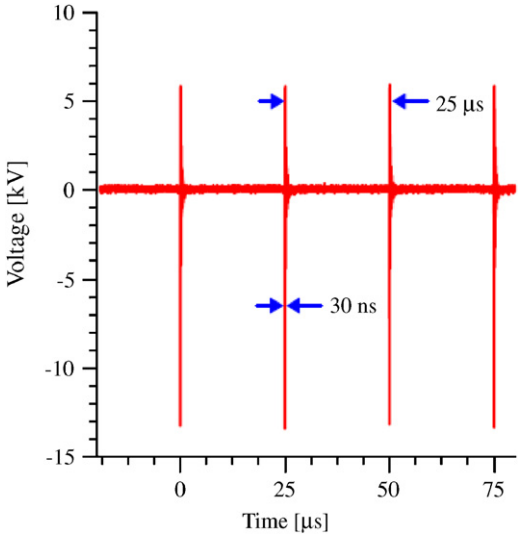

Fig. 14. Voltage oscillogram for 40 kHz pulsed ionization of a Mach 3 nitrogen flow. The test section pressure is 8.4 torr and $B = 1.5$ T (from [36]).

pulses measured from the ionization system operating at 40 kHz. Fig. 15 shows two current oscillograms measured from the DC Lorentz force circuit for the same conditions as Fig. 14, created with constant electrode potentials of 2 kV (one at each polarity). The current rises at the initiation of each ionization pulse, and then falls with the WIG decay. With slightly different test section conditions, a current oscillogram appears in Ref. [37] for an ionization frequency of 100 kHz, which results in a more constant Lorentz force over time because the WIG decays less. As one can see from Fig. 15, the Lorentz force system has an average power consumption of about 2 kW and it is capable of creating the pressure changes shown in Fig. 6.

3.5. Overall feasibility

A few examples of recent EMFC facilities have been presented in this section. These facilities have emphasized the use of electromagnetic forces within the boundary layer and they have shown that EMFC can have a considerable effect at supersonic and hypersonic flow speeds. However, the pressures at which these experiments have been conducted, as well as the magnitudes of σ and B, are far below what may be necessary for a hypothetical AJAX scramjet engine. Consequently, these systems are more applicable for boundary layer control of an aerodynamic surface or inlet system. Several steps must be taken to transition to a feasible electromagnetic virtual control surface. Experimental facilities have demonstrated success using low pressure core flows often surrounded by large magnets, and it is time to consider more compact configurations that can simulate environments like external flow over a wing or the beginning of an inlet compression system. In these environments, the magnets can be embedded below the surface and between the electrodes. Novel cooling methods must be developed for permanent magnets to survive the high-temperature environment. EMFC actuators may be placed in regions where the surface is actively cooled or is relatively cool. Considering the maximum operating temperature of rare-earth magnets, cooling to a temperature as low as 350 K may be necessary. Test section pressures must be increased, not necessarily to atmospheric, but perhaps to simulate the pressure after a shock over a thin wedge. The Mach 5 EMFC facility test section pressure reported by Shang et al. is meant to simulate an altitude from 30 to 50 km (0.6–7 torr) [40], but accounting for a real flight vehicle with a leading shock leads to much higher pressures in that altitude range (i.e., a 10° wedge at that speed would lead to a static pressure of 2–20 torr).

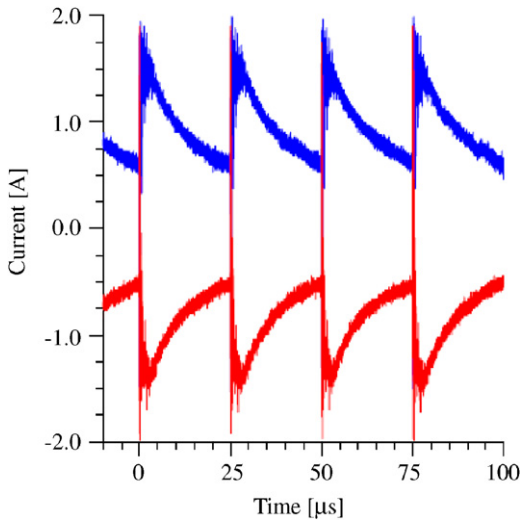

Fig. 15. Current oscillogram for Lorentz force power supply with the test conditions of Fig. 14 and different 2 kV electrode polarities (from [36]).

Although it appears challenging, experimental generation of a Lorentz body force is not particularly difficult for EMFC actuators. The key problem is creating non-thermal ionization to supply a conductive working fluid for the actuator [24]. Under rarefied conditions, DC ionization systems are capable of creating a diffuse WIG for which σ can reach a few $\mho$/m at high speeds. As pressure rises, the voltage required to sustain a glow discharge rises. This relationship makes arcing with DC discharges more probable for EMFC as charge builds up on the electrodes. High voltage, high-frequency pulsed ionization sources are another available method for creating the same value of conductivity. These discharges with high energy transfer during low duty cycle pulses can be applied in systems to produce non-thermal ionization, and σ is sustained by using a frequency fast enough to counteract the WIG decay.

Table 2
EMFC experimental environment summary.

Ref.	Year	Mach num.	σ ($\mho$/m)	p (torr)	B (T)	Magnet type	Ionization source	Medium	Configuration
[22]	1995	Low-speed	3.2	1300	≈ 0.4	NdFeB	N/A	Salt water	Flat plate
[41]	2002	5.8	1–2.5	1.2–2	0–2	Electromagnet	High voltage DC	Air	Blunt body
[30]	2002	4	≈ 0.01	6–8	≈ 0.4	NdFeB	High voltage RF	He, N_2	Channel
[12]	2002	4	0.05–0.1	2–10	0.45	NdFeB	High voltage RF	He	Channel
[32]	2003	3	0.02–0.12	12–15	0–1.5	Electromagnet	High voltage RF	N_2	Channel
[45]	2003	Low-speed	≈ 3	760	≈ 0.4	NdFeB	N/A	Salt water	Flat plate
[33]	2004	3.4	0.08–0.18	7–20	0–1.75	Electromagnet	High voltage RF	N_2, air	Channel
[43]	2005	5.1	≈ 1	0.6	0.1–0.2	Electromagnet	High voltage DC	Air	Flat plate
[34]	2005	3.4	0.14–0.23	7–20	0–1.5	Electromagnet	High voltage RF	N_2, air	Channel
[88]	2005	5.1	≈1	0.8	0.2	Electromagnet	HV, 10 Hz-RF	Air	Flat plate
[40]	2005	5	2	0.6–7	0–1	Electromagnet, NdFeB	HV DC, RF rad.	Air	Flat plate
[23]	2005	3	≈0.1	7–20	0–1.5	Electromagnet	High voltage RF	N_2, He	Channel
[28]	2005	3	≈ 0.07	7–20	0–1.5	Electromagnet	High voltage RF	N_2, He, air	Channel
[35]	2006	3	≈ 0.1	7–20	0–1.5	Electromagnet	High voltage RF	N_2, air	Channel
[38]	2006	2.8	N/A	28	0–2	Superconducting	Plasma column	Air	Channel
[36]	2006	3	≈ 0.1	7–20	0–1.5	Electromagnet	HV RF, seeding	N_2, air	Channel
[42]	2006	5.3	0.06	≈ 0.6	0–1	Electromagnet	High voltage DC	Air	Flat plate
[29]	2006	3	≈ 0.1	7–20	0–1.5	Electromagnet	High voltage RF	N_2, air	Channel
[86,87]	2007	2.8	N/A	28	0–4.5	Superconducting	Plasma column	Air	Wedge
[37]	2007	4	≈ 0.1	4.8	0–1.63	Electromagnet	High voltage RF	N_2	Channel
[39]	2008	2.6	N/A	28	0–4.5	Superconducting	Plasma column	Air	Wedge
[44]	2008	5.15	≈ 1	0.6	0–0.2	Electromagnet	High voltage DC	Air	Flat plate, inlet

Ionization sources for EMFC actuators should trend towards using RF or square wave signals, as long as the packaging of the pulsing circuit elements does not lead to size and weight requirements much greater than a DC system. Fridman et al. postulated that voltage pulse durations less than 100 ns/cm of anode and cathode separation can sustain streamers without transformation into arcs [90]. Refining that estimate and determining the plasma decay rate between pulses will allow for the optimization of the ionization source and will minimize fluctuations to the flow conductivity. The constant development of power semiconductors should make high-frequency pulsing systems smaller and more cost effective. Separate ionization and Lorentz force power supplies can be combined over the same flat plate electrodes with the use of rectifiers or diodes. The largest difference in pressure is obtained when the Lorentz force and Joule heating effectively work together. Since Joule heating thickens the boundary layer and decreases the local speed of sound, a Lorentz force applied to retard the freestream flow or direct it off of the surface has the greatest effect.

With these issues properly addressed, EMFC could potentially be used in place of traditional control surfaces at high altitudes. It should not be questioned if the Lorentz force is powerful enough to provide high-speed aerodynamic control. The main issue is the determination of whether or not the ionization and Lorentz force power requirements of an actuator result in a system compact enough to be implemented into a flight vehicle. Table 2 provides a summary of literature in this section with experimental environments highlighted.

4. Flow control by glow discharge

Although much of the previous discussion has been dedicated to flow control by electromagnetic fields, it must be noted that considerable interest for flow control with only plasma or electric fields has developed. Techniques for aerodynamic flow control by electric fields can be categorized into glow discharges and DBDs, covered in the next two sections, respectively. A glow discharge is formed across a gap of air or another gas between two electrodes with a difference in electric potential. The presence of a glow discharge is based on factors such as electrode geometry, ambient pressure, the gap medium, and the voltage. The glow discharge essentially means that the gap is filled with free radicals and electrons traveling between the electrodes. As such, the current increases rapidly after initial formation. Increasing the voltage after the glow discharge is formed eventually leads to electrical breakdown and arcing. A diffuse discharge is desirable since it indicates that the WIG effects will be uniform throughout the glow region. Often, experimentation with this phenomenon has occurred in low pressure environments where it is easier to create a diffuse discharge with a relatively low voltage. High pressure glows are also possible, and applying the potential difference with an increasing frequency has shown that the same current is maintained with a lower voltage [91].

Bletzinger et al. have provided a review of plasmas related to high-speed aerodynamics, containing a short history of the development of experimentation with glow discharges in recent decades [92]. In summary, initial shock tube experiments were conducted by measuring the drag and shock wave structure of objects (often blunt) while recording the differences with and without the actuation of a plasma source. As shown in Fig. 16, plasma flow as opposed to typical flow can drastically change the standoff distance of a bow shock around a blunt body [93]. Similar results were demonstrated as early as 1959 by Ziemer [94]. The change in shock wave geometry is important because a change in standoff distance can reduce heating and drag. Furthermore, the properties of a glow discharge may be used to improve the off-design performance of a high-speed inlet compression system by manipulating the shock wave structure. These features of glow discharges are significant for the future development of re-entry vehicles and hypersonic airbreathing propulsion. Although some of the early shock tube literature makes a case for electrohydrodynamic effects as the reason behind some of the shock wave alteration [95–97], the general consensus is that most of the effects seen are a product of the heating from the plasma [92]. Computational studies also indicate this result [98].

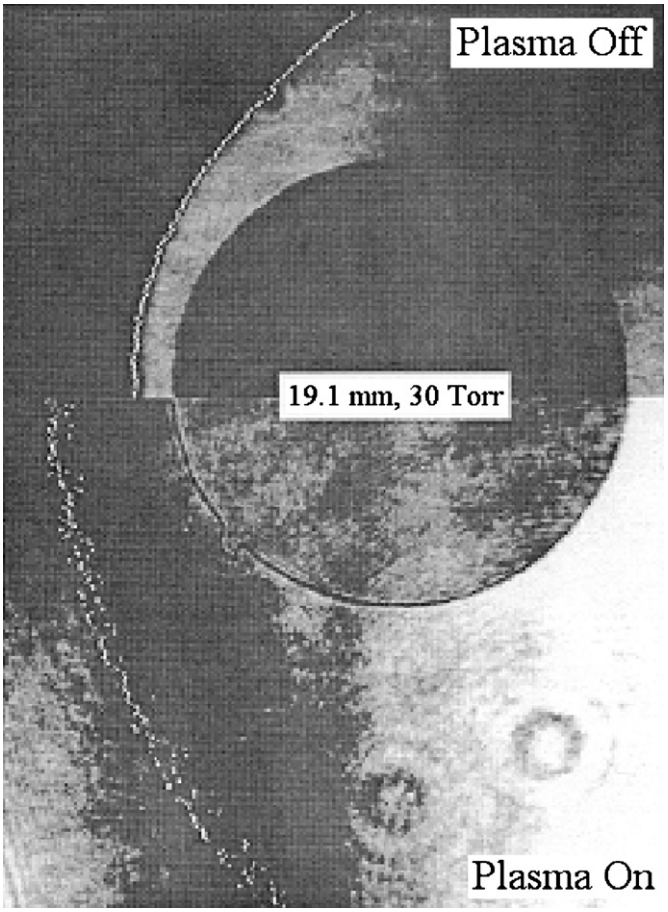

Fig. 16. Split image of a bow shock around a sphere with and without plasma for a flow velocity on the order of 1600 m/s (from [93]).

If the bulk of the glow discharge control effect is from heating, then the next logical step in the process of estimating its feasibility is to determine if there are benefits of plasma as opposed to other heating sources. One benefit of heating by glow discharges when compared to a typical heating element is rapid actuation. This may be a large enough benefit to continue experimentation with surface glow discharges for aerodynamic control. For instance, Shin et al. measured a glow discharge actuation time of less than 220 μs using pin electrodes on a flat plate in a Mach 2.85 flow environment [99]. This flat plate plasma actuator is capable of creating a weak shock wave over the actuator when the plasma is diffuse. A more constricted plasma formation in that environment, although produced with higher power, does not have the same shock wave control effect. The difference between plasma heating and surface resistance heating is noticeable, whereby the plasma has more of a volumetric effect and is not exclusively characterized as typical surface heating [100].

Flat plate experimentation with glow discharge plasma actuators for aerodynamic control has yielded promising results.

Experimental results from Ref. [100] show the plasma and surface heater both cause a 50% change in pitot pressure in Mach 5 flow over the cathode, with the glow discharge heater acting an order of magnitude faster. As was previously mentioned, the EMFC actuator in Ref. [43] produced an 18% change in lift while using only a DC glow discharge. Many other studies show similar results. Although efficiency improvements have been made, the performance of these plasma control systems is still uncertain across wide ranges of flight speeds and vehicle configurations [92]. If indeed the plasma effect is thermal and increases the local speed of sound, than it can intuitively be expected that the effect will be lessened as speeds increase and the post-shock air temperature and enthalpy increase. Hence, a flat plate actuator immersed in a low-temperature wind tunnel flow is a best case scenario for demonstrating glow discharge control. The power of the plasma source can be raised in order to compensate for a flow of higher enthalpy, but the efficiency of control may be drastically reduced. Experimental studies using plasma discharges with wedges and blunt bodies are discussed next to elaborate on this issue.

Although the presence of plasma can change the structure of a shock wave, it appears that most literature involving inlet compression systems also contains magnetic fields for the full Lorentz force effect. A detailed literature review appears in Ref. [92]. Some research with only plasma has been reported. For a Mach number of two and a flow mixture of nitrogen and helium, a glow discharge yielded a significant change in the oblique shock angle over a wedge [101]. The change in the shock angle indicates a change in the Mach number from 2 to 1.8 due to the plasma heating. The WIG source was located on the walls of the wind tunnel. Since the initial ramps of an inlet compression system are often not surrounded by an outer wall (e.g., X-43A design), it would be beneficial to test if this effect could be duplicated with a WIG source located entirely on the surface of the wedge. Placing a diffuse plasma source on the tip of a wedge and creating an effect on the oblique shock angle is a logical direction to move in to determine if these systems can be placed on a vehicle. Such a design was recently attempted by Gnemmi et al., where plasma discharges on a conical tip of a projectile were used to disturb a shock wave at freestream conditions of Mach 4.57 and 54 kPa static pressure [102]. More research is needed to determine if such systems can produce an appreciable aerodynamic control force, but it appears that ramp and inlet concepts of low to moderate turning angles are just as viable as flat plate concepts. Closely related to that design is the concept of a virtual cowl that can be created by plasma heating [103,104]. The plasma source is more likely to be high-energy electron beams or microwaves rather than glow discharges. The heat addition specifically can alter the upstream flowfield in order to reduce the inlet spillage. This concept will require a considerable amount of power to operate, but one must consider that any system with plasma heating may be used only during a (presumably short) transition process by acceleration to the design Mach number. Although most of these system designs are analytical models, some preliminary experimental studies have demonstrated the concept [105].

Concerning blunt bodies, many studies focusing on drag reduction have appeared in the literature. One initial study showed that the drag coefficient for a sphere in the presence of a WIG was significantly reduced for subsonic flow [106]. The same experiment for supersonic speeds showed that the drag coefficient was higher using a WIG than with typical airflow, attributed to an increase in the pressure integral on the front of the model at certain conditions. Other plasma sources constructed for drag reduction have proven to be more effective since then. Ganiev et al. reported a reduction in the drag coefficient of about 50% from Mach 0.59 to 4 using a plasma jet placed at the tip of a somewhat blunt body [107]. The reduction in the drag coefficient was found to depend on the stagnation temperature of the counterflow jet. Plasma jets appear to be inefficient for streamlined shapes [108]. At the time of Ref. [107], other publications also described drag reduction with plasma jets and other forms of focused energy addition. A thorough list of these can be found in Ref. [109]. However, the large drag reduction by the plasma jet injection appears to be more directly related to the counterflow jet instead of the thermal effects of the plasma. Fomin et al. experimentally determined that fluid dynamics instead of plasma is the dominant effect using the jet for moderate supersonic Mach numbers [110]. Those experiments were conducted using a truncated cone cylinder at Mach 2, 2.5, and 4. As was discussed, the use of plasma jets was eventually deemed unrealistic for MHD flight applications in the 1960s because of the power requirement. Many of these current systems have been met with enthusiasm, but again scaling the power requirements to flight vehicles or missiles may pose insurmountable problems with current technology. Although new publications continue to emerge with different plasma sources and test geometries, very little of it is predominantly different from what was carried out at the beginning of this decade.

Concerning the use of plasma flow control systems as part of realizable flight vehicles, some appear more feasible than others. In order to overcome problems including but not limited to power consumption, scaling, and hypersonic interaction at true flight conditions, the next step for plasma control for aerodynamics is a transition into realistic systems. It is understandable that some of the models of full-scale hypersonic systems have not been constructed due to the cost, but plasma control needs to be better proven experimentally as part of more flight-ready systems instead of basic shapes. Manipulating the bow shock wave around blunt bodies with plasma has been experimented with for 50 years, but no concrete applications are yet practical. It appears that ground testing of aerodynamic surfaces and inlet systems is moving forward, with the rapid plasma heating effect showing promise for control applications. The main challenge is producing systems that make use of current technology while maintaining power and packaging considerations.

5. Flow control by DBD

Considering the physics involved, a DBD is similar to a glow discharge. Where a glow discharge has an air gap, a DBD contains a gap of dielectric material between the anode and cathode. Typical materials like glass, polymers, and ceramics have a much higher resistivity than air, allowing for the electrodes to be placed closer to one another. Closer placement increases the electric field around the electrodes and ultimately raises the Coulomb force in Eq. (10) without the occurrence of electrical breakdown. The dielectric barrier is self-limiting as it prevents charge accumulation over the barrier material to prevent arcing. DBDs have been recognized since the mid-19th century, with the their first application being the production of ozone [111]. Since that time, research has continued to grow and now applications include surface treatment, reduction of pollutants, lasers, and plasma display panels. Systems using glow discharges often use low pressure, but these discharges were stabilized across the barrier at atmospheric pressure beginning in the 1980s [112].

DBDs constructed specifically for aerodynamic flow control applications appeared in the literature near the end of the 1990s [113,114]. In the decade since those reports, research into aerodynamic flow control with DBDs has rapidly increased both experimentally and computationally. A number of reviews have been written [51,115–117], which probably indicates a variety of

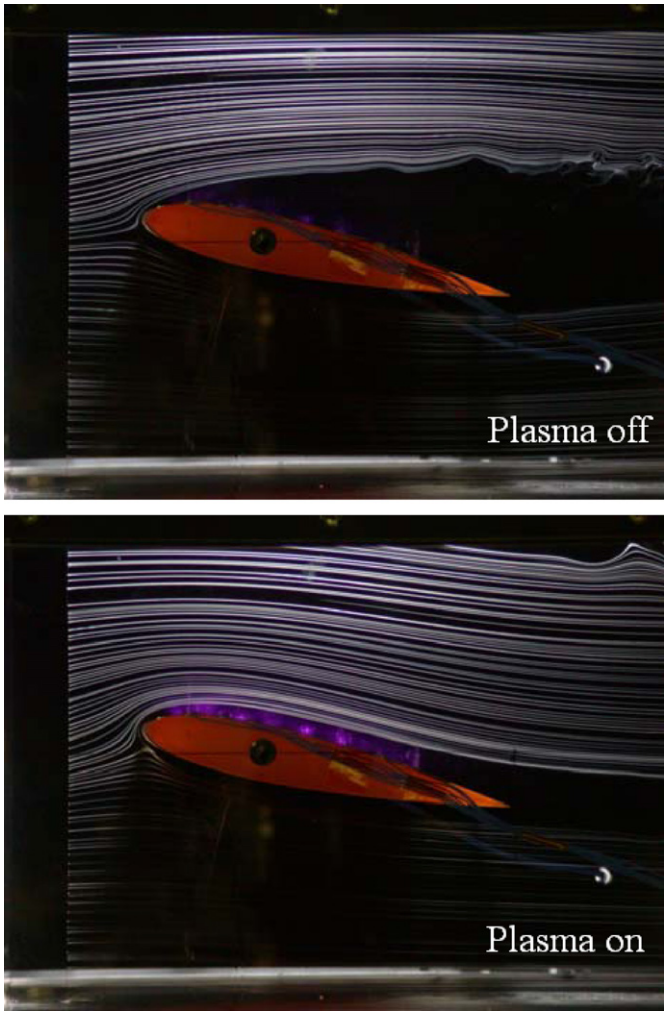

Fig. 17. Smoke visualization shows flow reattachment on a NACA 0015 airfoil at a 12° angle of attack by an array of EFC actuators. The freestream flow speed is 2.6 m/s (from [118]).

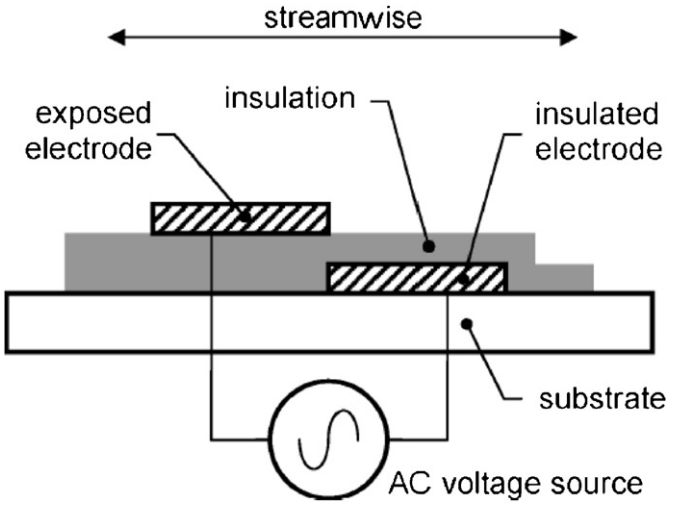

Fig. 18. Typical spanwise cross-section geometry of a dielectric barrier discharge actuator for aerodynamics applications (from [120]).

opinions on their applicability. Most conclude the DBD control effect is applicable for low Reynolds number flows below the general aviation range, and improvements to their strength will have to be made for them to be applied to flight aerodynamics. At low speeds, DBD actuators have a significant effect on boundary layer flow. Fig. 17 shows a notable image by Roth et al. of flow reattachment made possible by an array of DBD actuators [118]. This actuator system works at atmospheric pressure, and has been named the One Atmosphere Uniform Glow Discharge Plasma (OAUGDP™). The ionization is created with a high voltage RF signal and the barrier material is Kapton. An RF signal is used rather than a DC signal because it creates a cycle of charge exchange between the electrodes that increases the control effect. The waveform shape and frequency along with the dielectric material choice may be optimized to some extent, with many different configurations reported. Several studies with the system in Fig. 17 have resulted in successfully increasing or decreasing drag on a flat surface, adding momentum to the boundary layer flow, reducing the boundary layer thickness, and inducing a flow (also known as the ionic wind) of up to 6 m/s [119]. Fig. 17 raises the immediate question about the ability to apply a DBD system to high-speed flow where flow reattachment, drag reduction, and turbulence suppression are all major concerns. Although DBD actuators are studied by several institutions, the spanwise electrode geometry is always fairly similar and is depicted in Fig. 18 [120]. This linear arrangement also can be modified into an annular jet source (known as a plasma synthetic jet actuator), where pulsed operation can generate vortex rings [121]. The maximum jet velocity for that study was on the order of 1 m/s. The electrodes also may be wrapped around the internal diameter of an axisymmetric jet. Benard et al. demonstrated that this configuration may be used for jet mixing enhancement, where experiments increased mixing in a flow up to 30 m/s on a model with an exhaust diameter of 72.5 mm [122]. No modification was seen at a jet speed of 40 m/s. The self-limiting DBD allowed about 10 W of power to be transferred into the flow, and it was noted that this value must be increased for the DBD to have more effect on the jet flow.

The relative strength of current systems can be compared by their ability to induce a certain flow speed of air passing over the actuator. The ion wind speed measured in most recent surface DBD actuators is only a few meters per second, and efficient control results are obtained when u_∞ is less than 30 m/s [115]. However, some experiments have been conducted using higher freestream speeds. Opaits et al. [123] investigated DBD control of a NACA 0015 airfoil with freestream speeds of 20–75 m/s at atmospheric pressure. The stall angle was raised with the DBD actuators at $u_\infty = 75$ m/s, and a change in pressure distribution was also recorded. Similarly, Roupassov et al. [124] measured changes in the pressure distribution for a NACA 0015 airfoil at speeds up to 110 m/s. In this case, the electrodes were placed parallel to the flow, and it appears that the pressure distribution incurs a greater change with the DBD actuator when the airfoil is close it its stall angle. One attempt was made recently to mount a DBD actuator on the leading edge of the wing of a Jantar Standard SZD-48-3 sailplane [125]. It appears that the DBD system was able to affect the separation and lift characteristics of the wing surface, but the data collected were not particularly reliable and refined tests are needed. A study by Corke et al. stated a DBD actuator was able to excite three-dimensional boundary layer instabilities on a sharp cone at Mach 3.5, but no similar results have appeared since [126]. For current DBD actuators, it is clear that a speed of 30 m/s represents the freestream flow limit in which a noticeable control effect is demonstrated. For freestream speeds over 30 m/s, DBD actuators may slightly delay stall, assuming they are placed on the location where the flow will normally begin to separate.

In order to maximize DBD actuator performance for high-speed flow control, one may initially assume that the anode and cathode should have minimal size and be placed as close as

possible to each other and separated by a very thin layer of dielectric material. This geometry would maximize the electric field, where the Coulomb force grows with E^2 in Eq. (10). However, it has been argued that the force induced from DBD actuators should not be associated simply with E^2 and requires a more detailed analysis [127]. The ion wind is a momentum transfer between neutral particles and heavy ions whose motion is induced by the Coulomb force. Consequently, the electric field is significantly affected from the charge accumulation and particle interaction over the dielectric gap. This interaction dampens the electric field and is known as Debye or electrostatic shielding. Currently, numerical simulations are unable to simulate the observed random microdischarges in time and space that may help to resolve this issue. It does appear that the effectiveness of the exposed electrode is increased when it is thinner [120]. However, the ion wind increases with the width of the insulated electrode until it reaches a limit based on the applied voltage. Perhaps new efforts into geometric optimization or a method of resolving the E field dampening will yield a viable design for freestream flows of higher speeds. An increase in the ion wind speed would no doubt expand the usefulness of DBD actuators for aerodynamics. They may become capable of improving the efficiency of turbine blades as one example [128,129]. For those studies, DBD actuators were placed on the tip of low-speed turbine blades in a linear cascade. The chord Reynolds number was in the range of 10^4–10^5. An actuator placed close to the separation region of the blades was determined to have an effect similar to using tabular vortex generators, where the advantage of the DBD actuators is they are used only when necessary.

The lack of effectiveness of DBD actuators for higher freestream speeds is based more on the low energy input to the air flow rather than a reduction in the output ion wind due to electric field dampening. Going back to the work of Benard et al., axisymmetric jet mixing was achieved with DBD actuators for a Reynolds number limited to about 128,000 [122]. Similarly, axisymmetric jet mixing was obtained with RF frequency plasma actuators acting on a Mach 1.3 flow with a Reynolds number of approximately 1.1 million [130]. The RF frequency plasma actuators added considerably more energy to the flow at a rate of 160 W where the exit diameter was 25.4 mm. Several options are potentially available to raise the strength of DBDs. First, the potential difference could be raised between the DBD electrodes. Enloe et al. have estimated that the induced velocity increases with $V^{3.5}$ [120], but very high voltage DBD actuators with an ion wind speed over 6–8 m/s still have not been demonstrated. Increasing the voltage ultimately leads to greater instability and possible signal interference if actuators are eventually placed on aircraft. Conceivably, altering the barrier material may lead to a design with higher power input, but doing so may increasingly indicate that high frequency plasma actuators without any barrier material at all are more practical for high-speed flow control. Certainly attempts are being made to limit electrostatic shielding and increase DBD efficiency, but little discussion appears on a concrete methodology behind pursuing this strategy.

Without significant improvements to their overall strength, current DBD actuators are suited only for low Reynolds number aerodynamic control applications. A noticeable increase in work with applying DBD actuators to unmanned air vehicles (UAVs) and even MAVs has occurred in the past few years. One major issue with the development of small aircraft is the design of low Reynolds number airfoils that produce useful lift. Leading edge actuators have been demonstrated experimentally and computationally to increase the flight envelope of some familiar airfoil designs by modifying lift and drag [54,131,132]. DBD control for MAVs is advantageous for airfoils with high sweep and angle of attack where the use of conventional flaps and ailerons is either troublesome or completely ineffective. However, the effectiveness of low Reynolds number DBD active flow control actuators is very much dependent on the airfoil leading edge geometry [132]. These actuators are also limited to the low Reynolds number range because they lose their effectiveness in rarefied atmospheric pressure environments normally encountered by high-speed vehicles. Fortunately, a momentum transfer study by Abe at al. has shown that DBD actuator thrust actually increases for a certain pressure range below atmospheric [133]. Until pressure was reduced to about 60 kPa, the performance was greater than or equal to what was recorded for atmospheric pressure conditions. Afterwards, performance dropped as pressure was reduced further and sparks began to develop which damaged the barrier material. This study indicates the actuators should perform well to a flight ceiling of perhaps 5 km. The power requirement of these UAVs and MAVs appears again to be only on the order of tens of watts or less. The next logical step in the development of these systems is to determine the mass requirements of the actuator circuit. The scalability of the mass and volume requirements of DBD systems must be determined for potential integration into UAVs and MAVs. Although it is well known that DBDs are lightweight and compact enough to be placed on a thin airfoil, the same has not yet been verified for corresponding on-board high voltage transformer and control circuit elements.

6. Conclusions and future outlook

Flow control with electric or electromagnetic fields is an exciting topic due to its multidisciplinary nature, the possibility to solve difficult high-speed aerodynamics problems, and the overall design challenges. Also, another long-term factor can be added. It has long been theorized that research into new sources of atomic energy will eventually produce an extremely high power, yet compact generator system. The engine tested during Project Pluto shows that a nuclear reactor with 1960s technology was close to being capable of supporting a Lorentz force accelerator with thermal ionization. However, the radiation makes their implementation into a flight vehicle unacceptable. When a major breakthrough eventually happens, these new on-board generators will make all forms of MHD flow control realizable. Lorentz force engines may even someday replace conventional turbojet and ramjet engines. Until that time, an inquiry must be made as to what EFC and EMFC technologies can be supported with on-board power generators with today's technology. Thermal ionization for bulk flows does not appear achievable, leaving the non-thermal WIG sources as the best prospects for creating an appreciable amount of conductivity. Also, the flow speed range in which electromagnetic, glow discharge, and DBD systems are applicable does not appear to be clearly defined. Electromagnetic actuators are optimal for very high speeds where the flow downstream of the leading shock becomes ionized by itself and the thermal effect of using only plasma is likely to be negligible. This leaves a sizeable subsonic and supersonic gap where none of these concepts have been found to be relatively superior yet.

EMFC actuators can be characterized in more detail with a better use of dimensionless parameters. For MHD accelerators, reaching $I_M \approx 1$ is achievable. For control surfaces, reaching $I_M \approx 1$ requires extremely low pressures and unrealistic magnetic fields. However, reaching that value is not necessary for boundary layer EMFC. The parameter defined as I_{EM} may be more appropriate, not just because it results in a higher value but because it includes the electric field and more accurately depicts the contours of the Lorentz force. The use of one dimensionless number over the other is based on the MHD loading parameter which indicates if one Lorentz force term out of EB and uB^2 is dominant.

DBDs, because of their geometric simplicity and compact size, seem ideal for high-speed flow control. For years, their applications have been growing and DBDs can be found in most households and offices in plasma display panels. The concept of utilizing DBDs for aerodynamic control has existed for a little more than 10 years. Although this concept is under active research, it appears as though DBDs are limited to affecting freestream flow speeds of less than 30 m/s despite many optimization efforts to improve their strength. Limited control has been seen for speeds over 100 m/s when, for instance, the actuators are located directly where separation begins to occur over an airfoil. Therefore, current DBD actuators do not appear to be robust enough for all but very low-speed flight applications. The systems may be integrated into UAVs and other small vehicles to improve the airfoil flight envelope, but it is unclear if there will be a distinct advantage using this particular control concept due to the weight of on-board electrical circuits. The power requirement itself is low enough for small vehicles, but the supporting high voltage pulse equipment may lead to scaling problems. A tradeoff study should be considered for this issue.

While DBDs have generally been researched with atmospheric pressure and low speeds, glow discharge phenomena have operated in low pressure, high-speed environments. As was discussed, the effect of glow discharges is generally thermal, which changes the local Mach number and can affect drag and the shock wave geometry. Although glow discharges have demonstrated several capabilities during subscale ground tests, some of their trends may be troublesome for high-speed flight. For instance, the glow discharge thermal effect will likely be reduced for higher speeds which produce higher aerodynamic heating. However, the rapid actuation ability is desirable and has been experimentally demonstrated to produce a significant change in surface pressure. More emphasis should be placed on surface actuators and inlet systems in an effort to advance from blunt body testing which does not appear to have led to any engineering applications. Counterflow plasma jets do not appear to be practical with thermal ionization. Another area where plasma will make a major impact in aerodynamics is the use of actuators to assist ignition and combustion. Ref. [134] provides a thorough experimental review of that field.

It appears that EMFC actuators have considerable potential for further research into high-speed flow control. EMFC systems have one major disadvantage when compared to DBD and glow discharge control in that a separate ionization system is needed to generate conductivity for the Lorentz force to take effect for typical high-speed aerodynamic conditions. However, new methods of creating non-thermal conductivity by high-frequency pulsed discharges, electron beams, microwaves, radiation, and various combinations are promising. Increased research into improving the conductivity seen with these systems and operating with higher pressures is recommended. Also, proof-of-concept testing of these systems will lead to further understanding of their effectiveness for control surface implementation. Magnet selection is another critical issue. Inexpensive NdFeB magnets can be placed into thin control surfaces, but they may need considerable active cooling in hot aerodynamic environments. It is unknown if the field strength of these magnets will be high enough at this time. Electromagnets and superconducting magnets provide much higher surface fields than NdFeB magnets, but they carry a large weight penalty and must additionally be powered. Although NdFeB magnets have been discussed and tested to some extent in recent publications, more research should be conducted with them contained in compact control surface actuators. If NdFeB magnets prove to be powerful enough and can be cooled, the EMFC control should be more effective than control only with plasma. If not, plasma control with the rapid actuation effect becomes more advantageous.

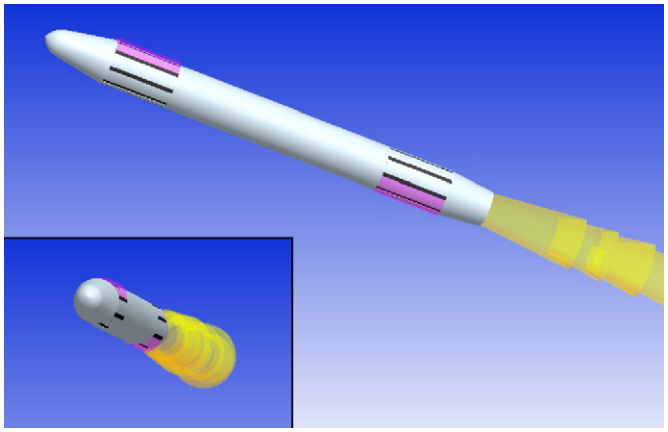

Fig. 19. Example of a future high-speed missile with EMFC actuators that could potentially replace conventional control surfaces. Magnets may be embedded beneath and between the electrodes (colored black) and diffuse plasma (colored purple) is observed when the controls are actuated.

Perhaps the best prospects for on-board EMFC with current technology are for improved control of high-speed missiles, which would benefit from surfaces that can actuate rapidly with reduced heating and drag when compared to mechanical actuators. A futuristic depiction is shown in Fig. 19. Power requirements will be raised, but improvements in on-board generators like state-of-the-art MEMS microturbines may be able to provide the same power input for 5% of the weight of current batteries [55]. With actuators creating a body force to control the direction of the missile, perhaps fins may even become unnecessary. Control may be initiated from many locations around the missile to maneuver it when segmented electrodes are placed around the diameter as shown. Magnets may be placed under the surface between the electrodes if EMFC is proven more effective than control only with plasma discharges.

As the fields stand now, active flow control with electromagnetic, glow discharge, and DBD actuators are at different phases of development. EMFC is the least developed, with much to be studied about its performance in simplified flow environments like channels, wedges, and flat plates. Flow control with glow discharges has been studied for decades with simple flow environments, but more detailed and improved concepts appear to be trending away from being applied to blunt bodies to being used for aerodynamic control surfaces. Control with DBDs is the most advanced of the three with detailed experimental analysis of both the physical aspects and integration into potential flight systems. All have major design hurdles to overcome before they can be labeled flight-ready technology, where perhaps the largest hurdle is the integration of the power supply and additional electric circuit components into a vehicle. However, technical needs coupled with demonstrations of the potential that exists with EMFC and EFC systems make the prospects for further research in this field promising.

Acknowledgments

The authors would like to thank Dr. J. Craig Dutton of the University of Illinois at Urbana-Champaign for many useful discussions regarding EFC and EMFC as well as Dr. Ramakanth Munipalli of HyPerComp, Inc., for providing a computational MHD code that has been used for the EMFC electric field calculations presented in this paper. The authors are also grateful to Dr. Joseph

Shang of Wright State University for providing helpful comments on the manuscript prior to publication in conference paper form. This work was partially supported by the Texas Advanced Research Program, Project no. 003656-0013-2006.

References

[1] Resler RL, Sears WR. The prospects for magneto-aerodynamics. J Aero Sci 1958;25(4):235–45, 258.
[2] Rittenhouse LE, Pigott JC, Whoric JM, Wilson DR. Theoretical and experimental results with a linear magnetohydrodynamic accelerator operated in Hall current neutralized mode. AEDC-TR-67-150, Arnold Air Force Station, TN, November 1967.
[3] Rosa RJ. Part one: shock wave spectroscopy. Part two: engineering magnetohydrodynamics. PhD dissertation, Cornell University, Ithaca, NY; 1956.
[4] Patrick RM. Magneto-hydrodynamics of compressible fluids. PhD dissertation, Cornell University, Ithaca, NY; 1956.
[5] Simmons GA, Nelson GL. Overview of the NASA MARIAH project and summary of technical results. AIAA 1998-2752, Albuquerque, NM; June 1998.
[6] Gurijanov EP, Harsha PT. AJAX: new directions in hypersonic technology. AIAA 1996-4609, Norfolk, VA; November 1996.
[7] Kuranov AL, Sheikin EG. Magnetohydrodynamic control on hypersonic aircraft under "AJAX" concept. J Spacecraft Rockets 2003;40(2):174–82.
[8] Macheret SO, Shneider MN, Miles RB, Lipinski RJ. Electron-beam-generated plasmas in hypersonic magnetohydrodynamic channels. AIAA J 2001;39(6):1127–38.
[9] Caledonia GE, Person JC, Hastings D. Ionization phenomena about the space shuttle. Report AFGL-TR-86-0045, Physical Sciences, Inc., Andover, MA; January 1986.
[10] Holt AC. Electromagnetic braking for Mars spacecraft. AIAA 1986-1588, Huntsville, AL; June 1986.
[11] Tanifuji T, Matsuda A, Wasai K, Otsu H, Yamasaki H, Konigorski D, et al. Expansion tube experiment of applied magnetic field effect on reentry plasma. AIAA 2008-1113, Reno, NV; January 2008.
[12] Palm P, Meyer R, Ploenjes E, Bezant A, Adamovich IV, Rich JW, et al. MHD effect on a supersonic weakly ionized flow. AIAA 2002-2246, Maui, HI; May 2002.
[13] Macheret SO, Shneider MN, Miles RB. Modeling of plasma generation in repetitive ultra-short DC, microwave, and laser pulses. AIAA 2001-2940, Anaheim, CA; June 2001.
[14] Shang JS. Recent research in magneto-aerodynamics. Prog Aerosp Sci 2001;37(1):1–20.
[15] Bruno C, Czysz PA, Murthy SNB. Electro-magnetic interaction in a hypersonic propulsion system. AIAA 1997-3389, Seattle, WA; July 1997.
[16] Park C, Mehta UB, Bogdanoff DW. Magnetohydrodynamics energy bypass scramjet performance with real gas effects. J Propul Power 2001;17(5):1049–57.
[17] Roth JR. Aerodynamic flow acceleration using paraelectric and peristaltic electrohydrodynamic effects of a one atmosphere uniform glow discharge plasma. Phys Plasmas 2003;10(5):2117–26.
[18] Sutton GW, Sherman A. Engineering magnetohydrodynamics. New York: McGraw-Hill; 1965.
[19] Harrington RF. Introduction to electromagnetic engineering. New York: McGraw-Hill; 1958.
[20] Ericson WB, Maciulaitis A. Investigation of magnetogasdynamic flight control. J Spacecraft Rockets 1964;1(3):283–9.
[21] Elsasser WM. Dimensional relations in magnetohydrodynamics. Phys Rev 1954;95(1):1–5.
[22] Henoch C, Stace J. Experimental investigation of a salt water turbulent boundary layer modified by an applied streamwise magnetohydrodynamic body force. Phys Fluids 1995;7(6):1371–83.
[23] Meyer R, Nishihara M, Hicks A, Chintala N, Cundy M, Lempert WR, et al. Measurements of flow conductivity and density fluctuations in supersonic nonequilibrium magnetohydrodynamic flows. AIAA J 2005;43(9):1923–9.
[24] Macheret SO, Shneider MN, Miles RB. Magnetohydrodynamic and electrohydrodynamic control of hypersonic flows of weakly ionized plasmas. AIAA J 2004;42(7):1378–87.
[25] Braun EM. Electromagnetic flow control: a review and development and testing of a compact actuator. Master's thesis, The University of Texas at Arlington, Arlington, TX; 2008.
[26] Celinski ZN, Fischer FW. Effect of electrode size in MHD generators with segmented electrodes. AIAA J 1966;4(3):421–8.
[27] D'Ambrosio D, Giordano D. Electromagnetic fluid dynamics for aerospace applications. Part I: classification and critical review of physical models. AIAA 2004-2165, Portland, OR; July 2004.
[28] Nishihara M, Jiang N, Rich JW, Lempert WR, Adamovich IV, Gogineni S. Low-temperature supersonic boundary layer control using repetitively pulsed magnetohydrodynamic forcing. Phys Fluids 2005;17(10).
[29] Nishihara M, Rich JW, Lempert WR, Adamovich IV, Gogineni S. Low-temperature $M = 3$ flow deceleration by Lorentz force. Phys Fluids 2006;18(8).
[30] Palm P, Meyer R, Bezant A, Adamovich IV, Rich JW, Gogineni S. Feasibility study of MHD control of cold supersonic plasma flows. AIAA 2002-0636, Reno, NV; January 2002.
[31] Kimmel RL, Gogineni S, Adamovich IV, Rich JW, Zhong X. Update on MHD control of supersonic/hypersonic boundary-layer transition. AIAA 2003-6924, Norfolk, VA; December 2003.
[32] Meyer R, McEldowney B, Chintala N, Adamovich IV. Measurements of electrical parameters of a supersonic nonequilibrium MHD channel. AIAA 2003-4279, Orlando, FL; June 2003.
[33] Nishihara M, Meyer R, Cundy M, Lempert WR, Adamovich IV. Development and operation of a supersonic nonequilibrium MHD channel. AIAA 2004-2441, Portland, OR; June 2004.
[34] Nishihara M, Jiang N, Lempert WR, Adamovich IV, Gogineni S. MHD supersonic boundary layer control using pulsed discharge ionization. AIAA 2005-1341, Reno, NV; January 2005.
[35] Nishihara M, Rich JW, Lempert WR, Adamovich IV. Low-temperature $M = 3$ flow deceleration by Lorentz force. AIAA 2006-1004, Reno, NV; January 2006.
[36] Nishihara M, Rich JW, Lempert WR, Adamovich IV. MHD flow control and power generation in low-temperature supersonic flows. AIAA 2006-3076, San Francisco, CA; June 2006.
[37] Nishihara M, Bruzzese J, Adamovich IV, Udagawa K, Gaitonde D. Experimental and computational studies of low-temperature $M = 4$ flow deceleration by Lorentz force. AIAA 2007-4595, Miami, FL; June 2007.
[38] Zaidi SH, Smith T, Macheret S, Miles RB. Snowplow surface discharge in magnetic field for high speed boundary layer control. AIAA 2006-1006, Reno, NV; January 2006.
[39] Kalra CS, Zaidi SH, Miles RB. Shockwave induced turbulent boundary layer separation control with plasma actuators. AIAA 2008-1092, Reno, NV; January 2008.
[40] Shang JS, Kimmel R, Hayes J, Tyler C, Menart J. Hypersonic experimental facility for magnetoaerodynamic interactions. J Spacecraft Rockets 2005;42(5):780–9.
[41] Shang JS, Hayes JR, Miller JH, Menart JA. Magneto-aerodynamic interactions in weakly ionized hypersonic flow. AIAA 2002-0349, Reno, NV; January 2002.
[42] Kimmel RL, Hayes JR, Menart JA, Shang JS. Effect of magnetic fields on surface plasma discharges at Mach 5. J Spacecraft Rockets 2006;43(6):1340–6.
[43] Menart J, Shang J, Atzbach C, Magoteaux S, Slagel M, Bilheimer B. Total drag and lift measurements in a Mach 5 flow affected by a plasma discharge and a magnetic field. AIAA 2005-0947, Reno, NV; January 2005.
[44] Shang JS, Huang PG, Yan H, Surzhikov ST, Gaitonde DV. Hypersonic flow control utilizing electromagnetic-aerodynamic interaction. AIAA 2008-2606, Dayton, OH; April 2008.
[45] Thibault JP, Rossi L. Electromagnetic flow control: characteristic numbers and flow regimes of a wall-normal actuator. J Phys D Appl Phys 2003;36(20):2559–68.
[46] Phillips OM. The prospects for magnetohydrodynamic ship propulsion. J Ship Res 1962;6:43–51.
[47] Way S. Electromagnetic propulsion for cargo submarines. J Hydronaut 1968;2(2):49–57.
[48] Takezawa S, Tamama H, Sugawawa K, Sakai H, Matsuyama C, Morita H, et al. Operation of the thruster for superconducting electromagnetohydrodynamic propulsion ship "Yamato 1". Bull Mar Eng Soc Jpn 1995;23(1):46–55.
[49] Proceedings of the international symposium on seawater drag reduction, Newport, RI, 22–23 July 1998. p. 357–425 [Turbulent drag reduction methods: electromagnetic drag reduction].
[50] Cott DW, Daniel VW, Carrington RA, Herring JS. MHD propulsion for submarines. CDIF External Report No. 2DOE-MHD-D140, Butte, MT; October 1988.
[51] Corke TC, Post ML. Overview of plasma flow control: concepts, optimization, and applications. AIAA 2005-0563, Reno, NV; January 2005.
[52] Roth JR, Sin H, Madhan RCM, Wilkinson SP. Flow re-attachment and acceleration by paraelectric and peristaltic electrohydrodynamic (EHD) effects. AIAA 2003-0531, Reno, NV; January 2003.
[53] Enloe CL, McLaughlin TE, VanDyken RD, Kachner KD, Jumper EJ, Corke TC. Mechanisms and responses of a single dielectric barrier plasma actuator: plasma morphology. AIAA J 2004;42(3):589–94.
[54] Jayaraman B, Lian Y, Shyy W. Low-Reynolds number flow control using dielectric barrier discharge actuators. AIAA 2007-3974, Miami, FL; June 2007.
[55] Fleeman EL. Tactical missile design, 2nd ed. Reston, VA: AIAA; 2006.
[56] Müller KH, Krabbes G, Fink J, Gruß S, Kirchner A, Fuchs G, et al. New permanent magnets. J Magn Magn Mater 2001;226–230(2):1370–6.
[57] Magnetic Materials Producers Association. Standard specifications for permanent magnet materials. MMPA Standard No. 0100-00, Chicago, IL; 2000.
[58] Liu J, Walmer M. Designing with high performance rare earth permanent magnets. In: Proceedings of the 18th international workshop on high performance magnets and their applications, Annecy, France, August 2004. p. 630–6.
[59] Williams AJ, Walls R, Davies BE, Marchese J, Harris IR. A study of thermal demagnetisation behaviour of Nd-Fe-B sintered magnets by a magnetic field mapping system. J Magn Magn Mater 2002;242–245:1378–80.

[60] Hadjipanayis GC, Liu J, Gabay A, Marinescu M. Current status of rare-earth permanent magnet research in U.S.A. J Iron Steel Res Int 2006;13(Suppl. 1):12–22.
[61] Liu JF, Walmer MH. Thermal stability and performance data for SmCo 2:17 high-temperature magnets on PPM focusing structures. IEEE Trans Electron Dev 2005;52(5):899–902.
[62] Liu J, Vora P, Dent P, Walmer M, Chen C, Talnagi J, et al. Thermal stability and radiation resistance of Sm-Co based permanent magnets. In: Proceedings of the space nuclear conference 2007, Paper 2036, Boston, MA, June 2007.
[63] Liu J, Vora P, Walmer M. Overview of recent progress in Sm-Co based magnets. J Iron Steel Res Int 2006;13(Suppl. 1):319–23.
[64] Kneller EF, Hawig R. The exchange-spring magnet: a new material principle for permanent magnets. IEEE Trans Magn 1991;27(4):3588–600.
[65] Zeng H, Li J, Liu JP, Wang ZL, Sun S. Exchange-coupled nanocomposite magnets by nanoparticle self-assembly. Nature 2002;420:395–8.
[66] Garrison GW. Electrical conductivity of a seeded nitrogen plasma. AIAA J 1968;6(7):1264–70.
[67] Jahn RG. Physics of electric propulsion. New York: McGraw-Hill; 1968.
[68] Giannini GM. The plasma jet and its application. Office of Scientific Research TN 57-520; 1957.
[69] Kantrowitz AR. Introducing magnetohydrodynamics. Astronautics 1958; 3(10):18–20, 74–7.
[70] Frost LS. Conductivity of seeded atmospheric pressure plasmas. J Appl Phys 1961;32(10):2029–36.
[71] BenDaniel DJ, Bishop CM. Nonequilibrium ionization in a high-pressure cesium–helium transient discharge. Phys Fluids 1963;6(2):300–6.
[72] Zukoski EE, Cool TA, Gibson EG. Experiments concerning nonequilibrium conductivity in a seeded plasma. AIAA J 1964;2(8):1410–7.
[73] Cool TA, Zukoski EE. Recombination, ionization, and nonequilibrium electrical conductivity in seeded plasmas. Phys Fluids 1966;9(4):780–96.
[74] Brederlow G, Hodgson RT. Electrical conductivity in seeded noble gas plasmas in crossed electric and magnetic fields. AIAA J 1968;6(7): 1277–84.
[75] Chu TK, Gottschlich CF. Temperature measurement of an alkali metal-seeded plasma in an electric field. AIAA J 1968;6(1):114–9.
[76] Schweitzer S. Tensor electrical conductivity of atmospheric cesium-seeded argon. AIAA J 1967;5(5):844–7.
[77] Viegas JR, Kruger CH. Effect of multispecies ionization on electrical conductivity calculations. AIAA J 1968;6(6):1193–5.
[78] Lu FK, Liu HC, Wilson DR. Electrical conductivity channel for a shock tube. Meas Sci Technol 2005;16(9):1730–40.
[79] Hacker BC. Whoever heard of nuclear-powered ramjets? Project Pluto at Livermore and the Nevada test site, 1957–1964. J Int Comm Hist Technol 1995;1:85–98.
[80] Nowak R, Kranc S, Porter RW, Tuen MC, Cambel AB. Magnetogasdynamic re-entry phenomena. J Spacecraft Rockets 1967;4(11):1538–42.
[81] Simmons GA, Nelson GL, Ossello CA. Electron attachment in seeded air for hypervelocity MHD accelerator propulsion wind tunnel applications. AIAA 1998-3133, Cleveland, OH; July 1998.
[82] Elliot DG. Magnetohydrodynamic power systems. J Spacecraft Rockets 1967;4(7):842–6.
[83] Messerle HK. Magnetohydrodynamic electrical power generation. New York: Wiley; 1995.
[84] Mickelsen WR. Auxiliary and primary electric propulsion, present and future. J Spacecraft Rockets 1967;4(11):1409–23.
[85] Becker RA. Thermionic space power systems review. J Spacecraft Rockets 1967;4(7):847–51.
[86] Kalra CS, Zaidi SH, Alderman B, Miles RB. Non-thermal control of shock-wave induced boundary layer separation using magneto-hydrodynamics. AIAA 2007-4138, Miami, FL; June 2007.
[87] Kalra CS, Zaidi SH, Alderman B, Miles RB, Murty YV. Magnetically driven surface discharges for shock-wave induced boundary-layer separation control. AIAA 2007-222, Reno, NV; January 2007.
[88] Menart J, Shang J. Investigation of effects caused by a pulsed discharge and a magnetic field in a Mach 5 flow. AIAA 2005-4783, Toronto, Ontario; June 2005.
[89] von Engel A. Ionized gases. London: Oxford University Press; 1955.
[90] Fridman A, Chirokov A, Gutsol A. Non-thermal atmospheric pressure discharges. J Phys D Appl Phys 2005; 38(2):R1–24.
[91] Cobine JD. Gaseous conductors: theory and engineering applications. New York: Dover; 1958.
[92] Bletzinger P, Ganguly BN, Van Wie D, Garscadden A. Plasmas in high speed aerodynamics. J Phys D Appl Phys 2005;38(4):R33–57.
[93] Lowry H, Stepanek C, Crosswy L, Sherrouse P, Smith M, Price L, et al. Shock structure of a spherical projectile in weakly ionized air. AIAA 1999-600, Reno, NV; January 1999.
[94] Ziemer RW. Experimental investigation in magneto-aerodynamics. ARS J 1959;19:642–7.
[95] Klimov AI, Koblov AN, Mishin GI, Serov YuL, Yavor IP. Shock wave propagation in a glow discharge. Sov Tech Phys Lett 1982;8(4):192–4.
[96] Gorshkov VA, Klimov AI, Mishin GI, Fedotov AB, Yavor IP. Behavior of electron density in weakly ionized nonequilibrium plasma with a propagating shock wave. Sov Tech Phys Lett 1987;57:1138–41.
[97] Klimov AI, Mishin GI, Fedotov AB, Shakhovatov VA. Shock wave propagation in a nonstationary glow discharge. Sov Tech Phys Lett 1989;15:800–2.
[98] Poggie J. DC glow discharge: a computational study for flow control applications. AIAA 2005-5303, Toronto, Ontario; June 2005.
[99] Shin J, Narayanaswamy V, Raja LL, Clemens NT. Characterization of a direct-current glow discharge plasma actuator in low-pressure supersonic flow. AIAA J 2007;45(7):1596–605.
[100] Menart J, Henderson S, Atzbach C, Shang J, Kimmel R, Hayes J. Study of surface and volumetric heating effects in a Mach 5 flow. AIAA 2004-2262, Portland, OR; June 2004.
[101] Merriman S, Ploenjes E, Palm P, Adamovich IV. Shock wave control by nonequilibrium plasmas in cold supersonic gas flows. AIAA J 2007; 39(8):1547–52.
[102] Gnemmi P, Charon R, Dupéroux JP, George A. Feasibility study for steering a supersonic projectile by a plasma actuator. AIAA J 2008;46(6):1308–17.
[103] Macheret SO, Shneider MN, Miles RB. Scramjet inlet control by off-body energy addition: a virtual cowl. AIAA 2003-32, Reno, NV; January 2003.
[104] Shneider MN, Macheret SO. Modeling of plasma virtual shape control of ram/scramjet inlet and isolator. J Propul Power 2006;22(2): 447–54.
[105] McAndrew B, Kline J, Fox J, Sullivan D, Miles R. Supersonic vehicle control by microwave driven plasma discharges. AIAA 2002-0354, Reno, NV; January 2002.
[106] Mishin GI. Experimental investigation of the flight of a sphere in weakly ionized air. AIAA 1997-2298, Atlanta, GA; June 1997.
[107] Ganiev YC, Gordeev VP, Krasilnikov AV, Lagutin VI, Otmennikov VN, Panasenko AV. Aerodynamic drag reduction by plasma and hot-gas injection. J Thermophys Heat Trans 2000;14(1):10–7.
[108] Batenin VM, Bityurin VA, Bocharov AN, Brovkin VG, Klimov AI, Kolesnichenko YuF, et al. EM advanced flow/flight control. AIAA 2001-0489, Reno, NV; January 2001.
[109] Suchomel CF, Van Wie D, Risha D. Perspectives on cataloging plasma technologies applied to aeronautical sciences. AIAA 2003-3852, Orlando, FL; June 2003.
[110] Fomin VM, Maslov AA, Malmuth ND, Fomichev VP, Shashkin AP, Korotaeva TA, et al. Influence of a counterflow plasma jet on supersonic blunt-body pressures. AIAA J 2002;40(6):1170–7.
[111] Kogelschatz U, Eliasson B, Egli W. From ozone generators to flat television screens: history and future potential of dielectric-barrier discharges. Pure Appl Chem 1999;71(10):1819–28.
[112] Okazaki S, Kogoma M, Uehara M, Kimura Y. Appearance of stable glow discharge in air, argon, oxygen, and nitrogen at atmospheric pressure using a 50 Hz source. J Phys D Appl Phys 1993;26(5):889–92.
[113] Roth JR, Sherman DM, Wilkinson SP. Boundary layer flow control with a one atmosphere uniform glow discharge surface plasma. AIAA 1998-328, Reno, NV; January 1998.
[114] Massines F, Rabehi A, Decomps P, Ben Gadri R, Sgur P, Mayoux C. Experimental and theoretical study of a glow discharge at atmospheric pressure controlled by dielectric barrier. J Appl Phys 1998;83(6):2950–7.
[115] Moreau E. Airflow control by non-thermal plasma actuators. J Phys D Appl Phys 2007;40(3):605–36.
[116] Corke TC, Post ML, Orlov DM. SDBD plasma enhanced aerodynamics: concepts, optimization and applications. Prog Aerosp Sci 2007;43(7): 193–217.
[117] Jayaraman B, Shyy W. Modeling of dielectric barrier discharge-induced fluid dynamics and heat transfer. Prog Aerosp Sci 2008;44(3):139–91.
[118] Roth JR, Madhan RCM, Yadav M, Rahel J, Wilkinson SP. Flow field measurements of paraelectric, peristaltic, and combined plasma actuators based on the one atmosphere uniform glow discharge plasma (OAUGDP). AIAA 2004-845, Reno, NV; January 2004.
[119] Roth JR, Dai X. Optimization of the aerodynamic plasma actuator as an electrohydrodynamic (EHD) electrical device. AIAA 2006-1203, Reno, NV; January 2006.
[120] Enloe CL, McLaughlin TE, VanDyken RD, Kachner KD, Jumper EJ, Corke TC, et al. Mechanisms and responses of a single dielectric barrier plasma actuator: geometric effects. AIAA J 2004;42(3):595–604.
[121] Santhanakrishnan A, Jacob JD. Flow control with plasma synthetic jet actuators. J Phys D Appl Phys 2007;40(3):637–51.
[122] Benard N, Bonnet JP, Touchard G, Moreau E. Flow control by dielectric barrier discharge actuators: jet mixing enhancement. AIAA J 2008;46(9): 2293–305.
[123] Opaits DF, Roupassov DV, Starikovskaia SM, Starikovskii AYu, Zavialov IN, Saddoughi SG. Plasma control of boundary layer using low-temperature non-equilibrium plasma of gas discharge. AIAA 2005-1180, Reno, NV; January 2005.
[124] Roupassov DV, Zavyalov IN, Starikovskii AYu. Boundary layer separation plasma control using low-temperature non-equilibrium plasma of gas discharge. AIAA 2006-0373, Reno, NV, January 2006.
[125] Sidorenko AA, Budovsky AD, Pushkarev AV, Maslov AA. Flight testing of a DBD plasma separation control system. AIAA 2008-0373, Reno, Nevada, January 2008.
[126] Corke TC, Cavalieri DA, Matlis E. Boundary-layer instability on sharp cone at Mach 3.5 with controlled input. AIAA J 2001;40(5):1015–8.
[127] Enloe CL, McLaughlin TE, Van Dyken RD, Kachner KD, Jumper EJ, Corke TC. Mechanisms and responses of a single dielectric barrier plasma. AIAA 2003-1021, Reno, NV; January 2003.
[128] Huang J, Corke TC, Thomas FO. Plasma actuators for separation control of low-pressure turbine blades. AIAA J 2006;44(1):51–7.

[129] Huang J, Corke TC, Thomas FO. Unsteady plasma actuators for separation control of low-pressure turbine blades. AIAA J 2006;44(7):1477–87.
[130] Samimy M, Kim JH, Kastner J, Adamovich I, Utkin Y. Active control of high-speed and high-Reynolds-number jets using plasma actuators. J Fluid Mech 2007;578:305–30.
[131] Patel MP, Ng TT, Vasudevan S, Corke TC, He C. Plasma actuators for hingeless aerodynamic control of an unmanned air vehicle. J Aircraft 2007;44(4):1264–74.
[132] Greenblatt D, Göksel B, Rechenberg I, Schüle CY, Romann D, Paschereit CO. Dielectric barrier discharge flow control at very low flight Reynolds numbers. AIAA J 2008;46(6):1528–41.
[133] Abe T, Takizawa Y, Sato S, Kimura N. Experimental study for momentum transfer in a dielectric barrier discharge plasma actuator. AIAA J 2008;46(9):2248–56.
[134] Starikovskaia SM. Plasma assisted ignition and combustion. J Phys D Appl Phys 2006;39(16):R265–99.